



Ultrasonic Levitation with Phased Arrays and the Xilinx Zynq Platform

Daniel Connolly-Taylor, William Beasley, Brenda
Gatush, Asier Marzo, Jose Nunez-Yanez

ABSTRACT

Acoustic levitation employs acoustic waves to suspend an object in air without any contact. This type of levitation has been widely used for the manipulation and transport of particles within the fields of biology, medicine, and physics, among other areas.

Although several methods exist for contactless handling, including magnetic, electric, optical, and aerodynamic, acoustic processing has the advantage of being material independent. Therefore, it can manipulate insulators or conductors, magnetic or non-magnetic objects, with the use of acoustic forces. Its applications range from cell manipulation, blood washing for lipids separation, and sample isolation before x-ray radiation of proteins, to crystallographic experiments and manufacturing of small electronic devices.

Acoustic levitation can be achieved using an ultrasonic phased array. The array consists of a group of transducer elements that are pulsed independently. Each pulsed element creates an acoustic wave front which combines with those created from other elements. By using the principle of phasing, a beam pattern is formed, focusing sound in a desired direction. The most common type of levitation uses a standing wave to permit the suspension of particles. A second form of levitation, known as near-field or squeeze film, can levitate objects in a short range.

This project investigates the ability of an FPGA-based system on chip to levitate small particles using a third method, referred to as single-beam or single-sided array levitation. In this case, an acoustic trapping mechanism is created by creating an acoustic shape that can hold a particle in place, without using a reflector.

Echo wave reception is also explored with the purpose of adding feedback to the system to make it responsive to external stimulus.

The project is a continuation of previous work carried out which achieved standing wave levitation, exploiting the hardware parallelism and high I/O pin count that FPGAs offer.

CONTENTS

Abstract.....	i
Acknowledgements.....	Error! Bookmark not defined.
Author's Declaration	Error! Bookmark not defined.
Contents.....	ii
List of Figures	iv
List of Tables	v
List of Equations.....	v
List of Acronyms.....	v
1. Introduction and Scope.....	7
1.1 Aim of the project	7
1.2 Objectives.....	7
2. Related Work	8
3. Background	10
3.1 Sound propagation.....	10
3.2 Ultrasonic Phased Arrays	11
3.2.1 Transducer element	11
3.2.2 Steering and focusing sound.....	11
3.2.3 Phased array parameters.....	12
3.2.4 Size of the focal point for a square array.....	14
3.3 Calculation of the Acoustic Radiation Force	14
3.4 Acoustic Levitation.....	16
3.4.1 Standing-wave acoustic levitation	16
3.4.2 Near-field acoustic levitation	18
3.4.3 Single-sided array levitation.....	18
3.4.4 Alternatives to levitation	20
4. Resources	21
4.1 Software	21
4.2 Hardware and Equipment.....	21
5. Implementation	22
5.1 Previous Work.....	22
5.1.1 Ultrasonic Phased Array PCB Circuit	23
5.1.2 System Design	24
5.1.3 Focal Point Width.....	25
5.2 Current Work	25

5.2.1	Acoustically Transparent Mesh Fixture.....	27
5.2.2	Twin-Trap Creation	28
5.2.2.1	Simulation in Ultraino platform	28
5.2.2.2	Twin-Trap Implementation in C application	30
5.2.3	Echo wave capture.....	31
5.2.3.1	XADC core in Vivado design	31
5.2.3.2	Enabling the XADC module in the SDx Environment	32
5.2.3.3	PCB modifications for echo reception	33
5.2.4	Speed of sound adjustment for temperature variation.....	35
5.2.5	Embedded C application in SDx environment	37
5.2.5.1	UART user interface	37
5.2.5.2	Particle Position Estimation	40
6.	Results.....	43
6.1	Implemented Design Details.....	43
6.1.1	FPGA Resources Utilization.....	43
6.1.2	FPGA Timing Summary.....	43
6.1.3	FPGA Power Consumption.....	44
6.1.4	Phased Array Power Consumption	44
6.2	Achieving Mid-Air Levitation.....	45
6.3	Particle transportation.....	46
6.4	Captured echoes	48
6.5	Particle position analysis.....	50
6.6	Echo amplitude test	51
6.7	System Response to the presence of objects	53
7.	Conclusions	54
8.	Future Work	55
9.	References	56
10.	Appendix	60
	Available supplementary .mov videos:.....	60

LIST OF FIGURES

Figure 1: Haptic feedback with ultrasonic and laser fields [19].....	9
Figure 2 : Compression (a) and rarefaction (b) of the medium [9].....	10
Figure 3: Propagation of sound [10]	11
Figure 4: Steering (a) and focusing (b) a sound beam [11].....	12
Figure 5: Matrix array [17]	13
Figure 6: Focal point in Cartesian plane [18]	13
Figure 7: Width of the focal point for a square array [20].....	14
Figure 8: Generation of the acoustic radiation force [21]	15
Figure 9: Model of monopole and dipole resonator for a Rayleigh wave [23].....	15
Figure 10: Standing wave acoustic levitation (a) and wave visualization with CO ₂ (b).....	16
Figure 11: Stable position near the pressure node (a). Acoustic streaming effect (b) [27]... ..	17
Figure 12: Near-field acoustic levitation [29]	18
Figure 13 : Amplitude fields for three types of traps [30]	19
Figure 14: Phase signatures of acoustic traps [30]	19
Figure 15: Zynq Evaluation and Development Board [34]	22
Figure 16: Previous setup using standing wave levitation.....	23
Figure 17: Coordinates on phased array.....	23
Figure 18: System block diagram	26
Figure 19: Vivado system structure	27
Figure 20: Acoustically transparent mesh fixture side and top views	27
Figure 21: Side and top views of twin trap amplitude field.....	29
Figure 22: Side and top views of twin trap phase field [35]	29
Figure 23: Acoustic twin-trap lateral forces.....	30
Figure 24: Acoustic twin-trap longitudinal force	30
Figure 25: AXI XADC core (a) and XADC configuration (b)	32
Figure 26: Exporting the hardware platform (a). Content of .hdl file (b)	33
Figure 27: PCB modifications	33
Figure 28: Original circuit.....	34
Figure 29: Modified circuit.....	34
Figure 30: Receiver inclined position	34
Figure 31: Speed and wavelength of sound with temperature	35
Figure 32: Phase shift variation with temperature	35
Figure 33: Focal point width variation with temperature	36
Figure 34: Pmod HYGRO sensor IP component (a) and sensor PCB (b) [38]	36
Figure 35: User interface menu (a). UART interface configuration (b)	38
Figure 36: User interface - Fixed coordinate option	38
Figure 37: User interface – Move in X-axis	38
Figure 38: User interface – Closed Loop System	39
Figure 39: User interface – Setting speed of sound and wavelength	39
Figure 40: User interface – Test speed of particle.....	40
Figure 41: Flow diagram of embedded C software application.....	42
Figure 42: Programmable Logic resource utilization	43
Figure 43: Design Timing Summary	43
Figure 44: FPGA Power Report Summary	44
Figure 45: On-Chip component power consumption	44
Figure 46: Polystyrene sphere levitating above an acoustically transparent mesh	45

Figure 47: Mid-air levitation of polystyrene sphere (side view)	45
Figure 48: Diameters of levitated particles.....	46
Figure 49: Stable levitating area for a 4 mm particle.....	46
Figure 50: Translation of 4 mm sphere along Y axis with 1 mm step size (top view).....	46
Figure 51: Levitated 4 mm particle maximum speed	47
Figure 52: Echo waves for X coordinate 62 to 70 and Y coordinate 66	48
Figure 53: Echo waves for X coordinate 66 and Y coordinate 62 to 70	49
Figure 54: Particle position statistical analysis along the X-axis	51
Figure 56: Carboard (a) and foam (b) squares for echo amplitude test	52
Figure 57: Echo test setup with carboard and foam squares	52
Figure 58: Echo amplitude for different material sizes.....	53
Figure 59: System response to presence of objects	54

LIST OF TABLES

Table 1: Acoustic levitation conditions for solid samples	17
Table 2: Acoustic levitation conditions for liquid samples	17
Table 3: Levitation technologies [28].....	20
Table 4: Software Resources.....	21
Table 5: Hardware Resources	21
Table 6: Probable X coordinate within ADC sample number range	51
Table 7: List of available videos	60

LIST OF EQUATIONS

Equation 1: Aperture size along X and Y.....	13
Equation 2: Distance calculation from transducer element to focal point.....	14
Equation 3: Propagation time from transducer element to focal point.....	14
Equation 4: Focal point main lobe width [20].....	14
Equation 5: Acoustic potential energy.....	15
Equation 6: Scattering coefficients	15
Equation 7: Acoustic radiation force.....	16
Equation 8: Focal point width for the phased array used.....	25
Equation 9: Phase shift calculation for transducers U0 to U31	30
Equation 10: Phase shift calculation for transducers U32 to U63	31
Equation 11: Speed of sound with temperature variations [37]	35
Equation 12: Distances between the particle and each echo receiver.....	40
Equation 13: Calculation of X and Y coordinates with geometrical method	41

LIST OF ACRONYMS

FPGA	Field Programmable Gate Array
ZedBoard	Zynq Evaluation and Development Board
RTL	Register Transfer Level
FMC	FPGA Mezzanine Card
PCB	Printed Circuit Board

SWAL	Standing-Wave Acoustic Levitation
NFAL	Near-Feld Acoustic Levitation
AXI	Advanced eXtensible Interface
BRAM	Block Random Access Memory
FF	Flip-Flop
HLS	High-Level Synthesis
IDE	Integrated Development Environment
LUT	Lookup Table
SDK	Software Development Kit
SOC	System on a Chip
VHDL	Very High Speed Integrated Circuit Hardware Description Language
MOSFET	Metal Oxide Semiconductor Field-Effect Transistor

1. INTRODUCTION AND SCOPE

1.1 Aim of the project

The aim of this project is the investigation of how a custom driver board based on an FPGA system on chip (SoC) can be used for controlling an ultrasonic phased array with the purpose of performing acoustic levitation. An FPGA-based approach has been selected to take advantage of its inherent hardware parallelism, which will be useful for independently driving each transducer element. Additionally, the high I/O pin count this technology offers is also beneficial when using a large phased array.

Standing wave levitation has been previously achieved with the hardware setup proposed, so this project intends to enhance the previous work by also attaining single-beam levitation. The main difference being that the new system will not require a reflector plate to trap the levitated object. Instead, a trapping mechanism will be generated only by manipulation of the signals driving the transducers.

Feedback will be introduced by monitoring echo waveforms reflected to the array. This will allow the system to become responsive to external stimulus. Position estimation of the levitated object will also be explored.

1.2 Objectives

To achieve the tasks described, the following objectives are intended to be progressively met:

- 1) Obtain an overview of the ultrasonic phased array technologies and previous related work.
- 2) Review and replicate the previous work carried out with the setup in hand to obtain standing wave levitation of small particles.
- 3) Remove the reflector plate to observe the response of the particles when not in the presence of a standing wave and investigate ways to achieve mid-air single-beam levitation.
- 4) Add echo wave reception by including an ADC module in the previous design and incorporate receivers to the system to capture echoes being reflected from the levitated particle.

2. RELATED WORK

Ultrasonic phased arrays have a wide range of applications, including acoustic imaging for clinical analysis within the medical sector. They can also be used to evaluate the properties of materials using non-destructive testing to identify defects and perform failure analysis. Imaging may also be used for the study of underwater environments.

Other applications include mass measurement estimations using acoustic vibration, as well as non-contact transport of substances, mixing and dispensing. The term “acoustophoresis” is used to refer to the migration of particles using sound. It is widely used in the fields of biology and medicine, as it allows handling of particles in a gentle, label-free, and purely mechanical manner. For example, microfluidic separation chips, also referred to as Lab on a Chip, can make use of ultrasonic transducers placed underneath them to receive a standing wave that is perpendicular to the flow channel. This has the benefit of visually inspecting the separation efficiency of the particles [1].

Some innovative uses are haptic technologies with ultrasonic waves to recreate the sense of touch. These are useful to assist in the creation of virtual reality using 3D haptic shapes, for example, for the gaming sector. In [2] a method for creating volumetric haptic shapes that can be felt using focused ultrasound is proposed. An experiment was performed with a small group of users to test the method, with high accuracy results obtained. One of the drawbacks observed was the need for creating haptic shapes only within the working volume of the device. The device loses power as the user’s hand is removed from the active region. There is also a trade-off between the size and power of the transducer array and the number and strength of control points.

Aerial haptic feedback is also explored but in this case ultrasonic and laser light fields are combined to improve the user experience in virtual and augmented realities. In this application, a PC sends the coordinate of the focal point and required force to an FPGA. The FPGA calculates adequate time delays for each transducer in a phased array and generates the driving signals. The ultrasonic output force is varied to find the perceptual threshold, when it is possible to feel the haptic objects. The ability to distinguish between different shapes is discussed, for applications such as an aerial braille alphabet [3].

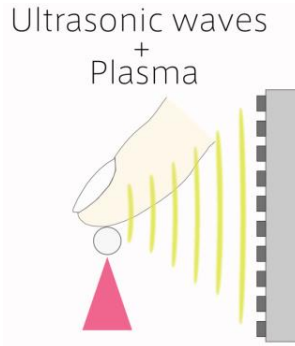


Figure 1: Haptic feedback with ultrasonic and laser fields [19]

A tactile display, called the Airborne Ultrasound Tactile Display (AUTD), has been created to produce tactile stimulation from a distance. The display makes use of airborne ultrasound to stimulate human skin. It uses the phased array focusing technique to produce radiation pressure that can press human skin in the direction of propagation. This technology is expected to provide tactile feedback to floating image displays and other user interfaces [4].

Amorin et al present a reconfigurable, cost-effective FPGA and PC-based ultrasonic system, designed for teaching and medical imaging research. The system uses the MD2131 beamformer source driver from Microchip Technology Inc. to generate arbitrary waveforms and an analogue frontend to obtain maximum flexibility and data access to various ultrasonic data streams. The results obtained from applications such as plane wave excitation and delay-and-sum beamforming show that the open platform can help biomedical students and researchers to develop and evaluate different imaging strategies for medical ultrasonic imaging and non-destructive testing techniques [5].

A comparison of FPGAs versus other technologies like DSPs and microcontrollers is addressed in [6], pointing out the ability of FPGAs to perform operations in less number of cycles as a result of dedicated hardware that can run operations in parallel and can be adjusted without needed to reprint the circuit board designed. A platform has been implemented that can test ultrasonic signal processing algorithms, based on the Microblaze 32-bit soft-core RISC processor and the Xilinx Embedded development kit (EDK) for software development.

Two embedded processing platforms, the Xilinx Virtex-5 FPGA using the MicroBlaze processor and a Xilinx Zynq FPGA with embedded ARM processor are compared in [7]. The study includes the implementation of signal processing techniques for ultrasonic imaging and non-destructive testing applications. Based on the execution times obtained with each platform, it is proven that Zynq FPGA with an ARM processor can compute ultrasonic algorithms up to 30 times faster than the Virtex-5 FPGA with a MicroBlaze processor.

An electromechanical system with a fast, adaptive digital control has been created to allow for near-field acoustic levitation. By controlling the actuator's vibration pattern of standing and travelling waves, a levitated object can be manipulated by air pressure only. A resonance tracking system is employed to keep the system within its resonance bandwidth [8].

3. BACKGROUND

3.1 Sound propagation

Sound is a pressure wave created as a result of a vibration that is transmitted through an elastic medium, most commonly air. An elastic medium will tend to return to its original shape after it is deformed when a force is applied to it. An example of an object with this characteristic is a spring. It can be thought of air as a collection of particles that are connected to one another by springs, with the springs representing the restoring forces associated with the elasticity of the medium [9].

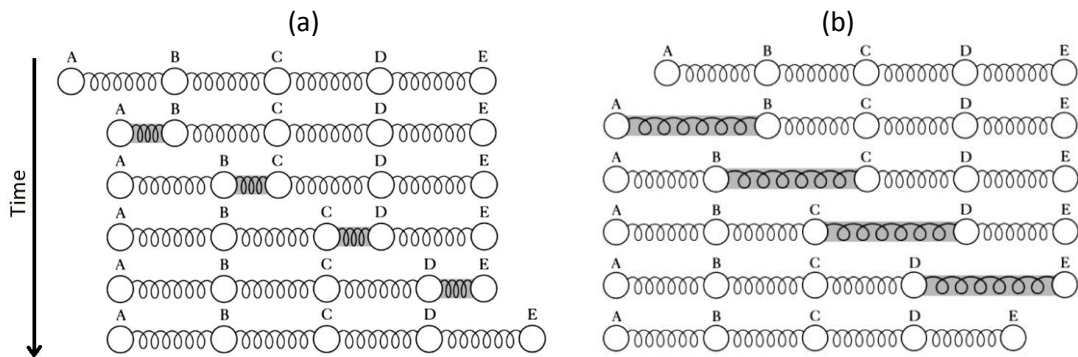


Figure 2 : Compression (a) and rarefaction (b) of the medium [9]

Figure 2(a), shows how pushing particle A towards B results in a compression of the spring and an increase in air pressure. Particle B will move to the right, increasing the force on the spring between B and C. The compression will continue to travel to the right along the springs between particles.

In the same manner, pushing particle A away from B causes the spring to stretch, and the tension generated in the spring will move particle B to the left. The resulting effect in which particles are separated further than normal and air pressure is lower than the atmospheric pressure is called rarefaction. Figure 2(b) shows how rarefaction travels to the right from one particle to the next [9].

When an object vibrates, the vibration moves along the line of particles while the particles only move back and forth from their fixed resting position. The distance between two

subsequent compressions is called the wavelength, and it corresponds to how much the wave has travelled in one cycle.

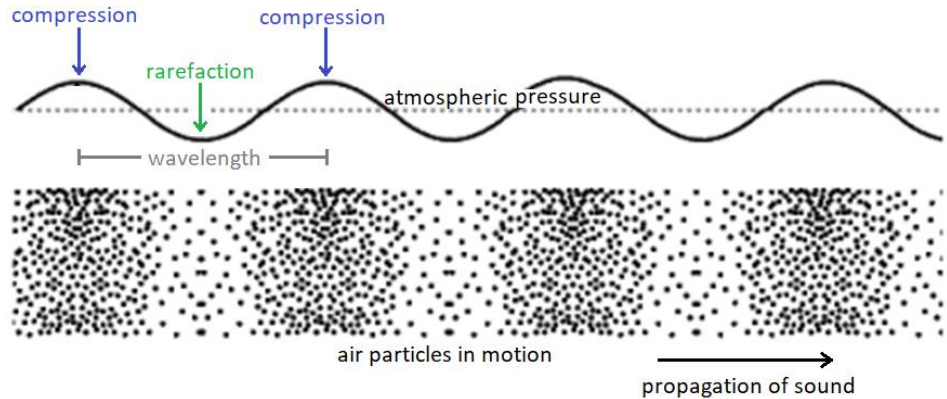


Figure 3: Propagation of sound [10]

3.2 Ultrasonic Phased Arrays

3.2.1 Transducer element

An ultrasonic transducer is commonly made of a piezoelectric material that converts electrical energy into mechanical motion of the element and vice versa. Therefore, when it is excited by an electrical pulse, a pulse of sound will be generated that will travel through a fluid in the form of an acoustic wave. If that wave hits an object and is reflected, some of the acoustic energy may return to the transducer, where it will be converted into electrical energy that is output as a voltage. It is possible to calculate the distance from the transducer to the object by knowing the speed of the wave and time of arrival of the pulse [11].

3.2.2 Steering and focusing sound

A phased array consists of a group of ultrasonic transducer elements which can be pulsed independently to create a specific beam pattern, focusing sound in a desired direction. As explained in [12], it uses the principle of phasing, varying the time between a series of outgoing ultrasonic pulses. Each element that is pulsed creates a wave front which combines with those created from other elements, adding, or cancelling their energy.

In the case where all elements are pulsed at the same time, the resultant wave front is planar and parallel to the transducer surface. To steer the beam, if the pulse for each element is delayed by a constant period after the previous element, the transmitted wave front will propagate at an azimuthal steering angle. It is also possible to obtain beam focusing along the axis perpendicular to the array, by creating delays that are mirrored symmetrically around the central element [13]. To do so, the transducers need to be pulsed starting from

the elements that are further away and moving inwards so that the closest elements are pulsed last.

The two parameters required to focus an array are the delays and the gain of each element. The set of delays is called “delay law”, and the set of gains is called “amplitude law”. Both form a single “focal law” [14].

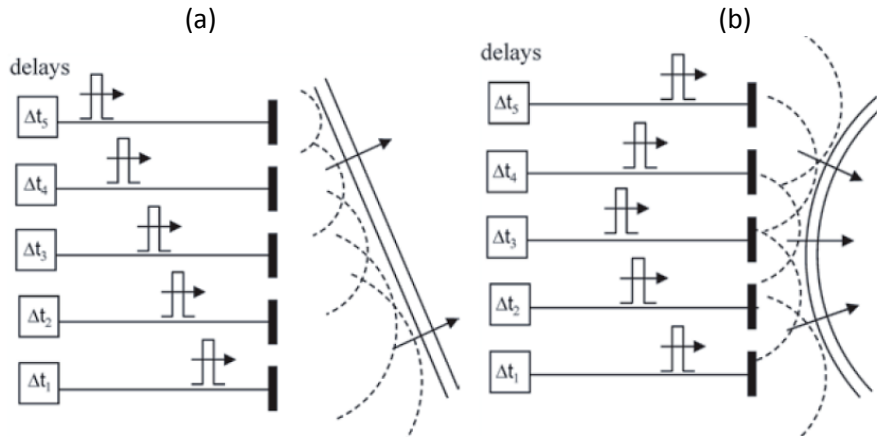


Figure 4: Steering (a) and focusing (b) a sound beam [11]

3.2.3 Phased array parameters

The beam pattern varies according to the following phased array parameters:

a) Frequency of operation:

The acoustic waves generated have higher frequencies than the human hearing threshold, located at 20 KHz.

b) Configuration:

Phased arrays are classified into one-dimensional (1-D) arrays, which can steer and focus beams on a plane, and two-dimensional (2-D) arrays, which can manipulate beams in a 3-D volume. Examples of 1-D include linear and annular arrays. Examples of 2-D include matrix and segmented annular arrays [15].

c) Number of elements:

Commonly between 16 and 128 elements per array, with some having as many as 256. The benefit of having a larger group is that it increases the ability to focus and steer the beam, and can increase the area coverage as well. The disadvantage is that having a higher density of “control points” within the same area reduces the strength that each individual element provides [2].

d) Pitch:

It refers to the distance between the centers of two adjacent elements. It should be less than one ultrasound wavelength to eliminate unwanted side lobes, which are caused by any sound energy that spreads out from the transducer at angles other than the primary path [16].

e) Element width:

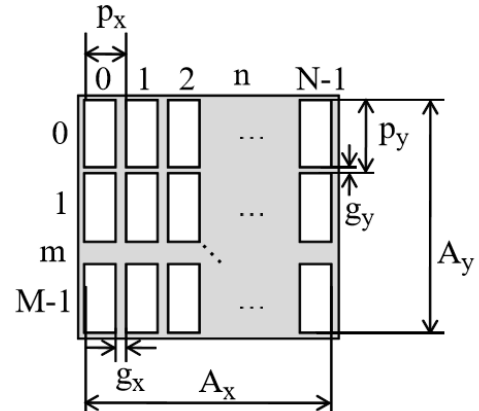
A smaller element width allows for better beam steering capability. There will be no side lobes when the element size is smaller than half a wavelength.

f) Aperture size:

For a matrix array, it is expressed as a function of the element pitch “ p ”, element gap “ g ”, and element number “ N, M ”, and is calculated as follows:

$$A_x = (N)(p_x) - g_x$$

$$A_y = (M)(p_y) - g_y$$



Equation 1: Aperture size along X and Y

Figure 5: Matrix array [17]

The figure below presents an array that is located in the $(x, y, 0)$ plane, and a focal point F is chosen at (x_j, y_j, z_j) . The azimuth steering angle is ϕ_j and the elevation steering angle is Θ_j .

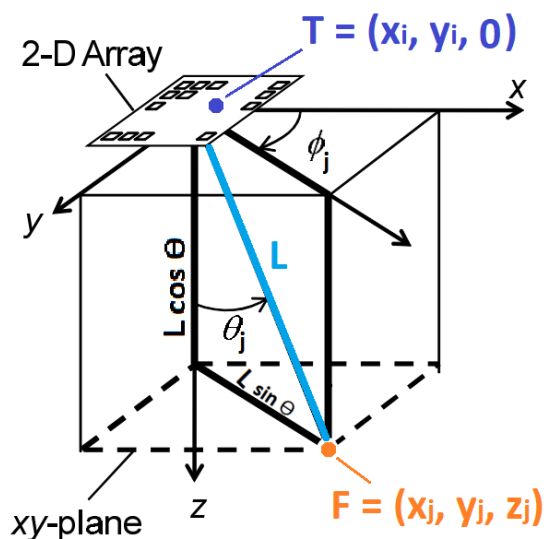


Figure 6: Focal point in Cartesian plane [18]

Using the Pythagorean theorem, the distance L from a transducer element T to the focal point F is defined as:

$$L = \sqrt{(x_j - x_i)^2 + (y_j - y_i)^2 + (z_j)^2}$$

Equation 2: Distance calculation from transducer element to focal point

It is possible to calculate the propagation time t_{ij} from the transducer element to the focal point F considering the acoustic propagation velocity c , as follows:

$$t_{ij} = \frac{L}{c}$$

Equation 3: Propagation time from transducer element to focal point

3.2.4 Size of the focal point for a square array

The spatial distribution of ultrasound generated from a square transducer array nearly has a sinc function shape. The width of the main lobe w , equivalent to the diameter of the focal point, can be expressed in terms of the sound wavelength λ , the focal length R , and the length of the side of the array D [20].

$$w = 2\lambda \frac{R}{D}$$

Equation 4: Focal point main lobe width [20]

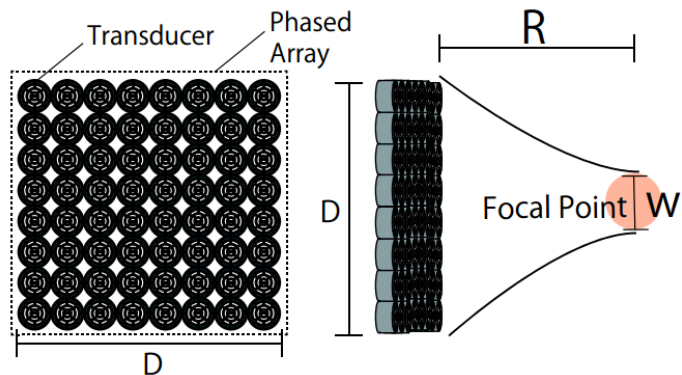


Figure 7: Width of the focal point for a square array [20]

3.3 Calculation of the Acoustic Radiation Force

Lev Gor'kov determined the average force that acts on a particle in an acoustic field, when the size of the particle is much smaller than the sound's wavelength. This force results from a non-uniform flux of momentum in the near-field region around the particle. It is the result

of incoming acoustic waves and the scattering on the surface of the particle when acoustic waves propagate through it [21].

Wave scattering by objects that are small compared to the wavelength is referred to as Rayleigh scattering [22].

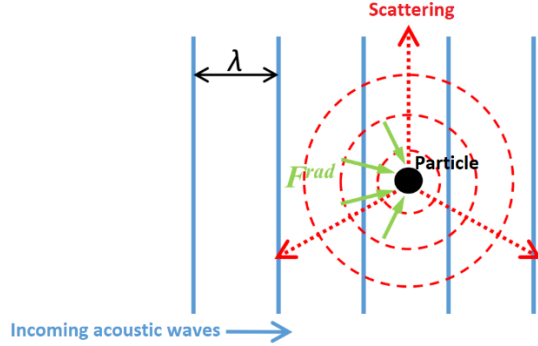


Figure 8: Generation of the acoustic radiation force [21]

The acoustic potential energy is calculated as follows [21]:

$$U = V_o \left(\frac{\overline{p_{in}^2}}{2\rho_f c_f^2} \cdot f_1 - \frac{3p_f \overline{v_{in}^2}}{4} \cdot f_2 \right)$$

Equation 5: Acoustic potential energy

The f_1 and f_2 coefficients below represent, respectively, the monopole and dipole resonators modelled as two spring-mass systems, used to evaluate the Rayleigh scattering effect [23]:

$$f_1 = 1 - \frac{\rho_f c_f^2}{\rho_p c_p^2} \quad f_2 = \frac{2(\rho_p - \rho_f)}{2\rho_p + \rho_f}$$

Equation 6: Scattering coefficients

where

- V_o is the volume of the particle
- p_{in} is the acoustic pressure
- v_{in} is the velocity of acoustic particles
- ρ_f is the density of the fluid
- ρ_p is the density of the particle
- c_f is the speed of sound in the fluid
- c_p is the speed of sound in the particle

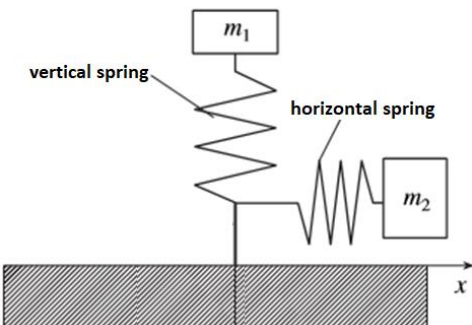


Figure 9: Model of monopole and dipole resonator for a Rayleigh wave [23]

The acoustic radiation force is the result of a combination of incident and reflected waves, and can be found by differentiation of the potential energy U :

$$F_{rad} = -\nabla U$$

Equation 7: Acoustic radiation force

3.4 Acoustic Levitation

The most studied types of levitation are standing-wave acoustic levitation (SWAL) and near-field acoustic levitation (NFAL). In recent years, a third type, referred to as single-beam or single-sided array levitation, using acoustic traps has been achieved.

Acoustic levitation employs acoustic waves travelling through a fluid, most commonly air, to suspend an object. These waves counteract the gravitational force, resulting in a floating action.

3.4.1 Standing-wave acoustic levitation

SWAL requires a transducer and a reflector. The transducer generates a sound wave that travels perpendicular to its angle of incidence until it reaches the reflector, bouncing back towards the source. An interaction between compressions and rarefactions causes sound interference [24]. This may lead to the creation of a standing wave.

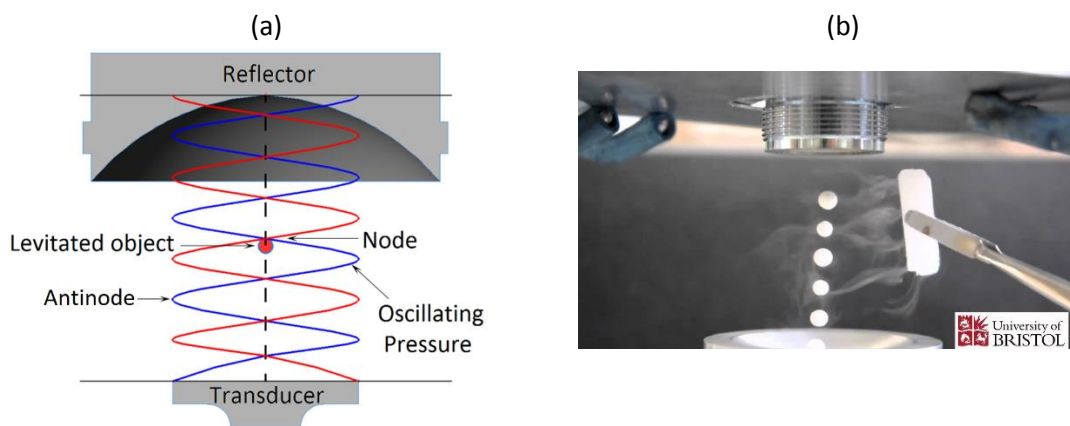


Figure 10: Standing wave acoustic levitation (a) and wave visualization with CO₂ (b)

When a compression meets another compression, they will combine to have twice the amplitude. A rarefaction that meets another rarefaction will combine in the same manner. In the case where a compression meets a rarefaction, they will both cancel each other, leaving the medium in equilibrium [25].

The areas of minimum pressure in a standing wave are called nodes. And those of maximum pressure are called antinodes. Floating particles will be suspended just below the

nodes, where the amount of pressure that a sound wave exerts on a surface balances the pull of gravity [24].

The figure below shows how a particle is capable of levitating on a standing wave as a result of axial radiation pressures and radial Bernoulli stresses. It can also be observed that when a fluid medium vibrates in contact with a solid, an acoustic streaming effect occurs due to friction between them [26].

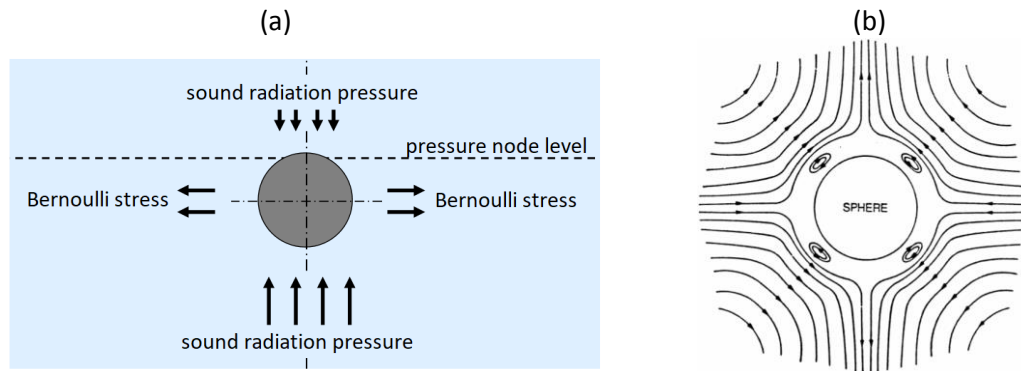


Figure 11: Stable position near the pressure node (a). Acoustic streaming effect (b) [27]

Standing wave levitation has the limitation that the object's diameter must not be greater than half of the wavelength of the acoustic waves. Tables 1 and 2 lists the limiting conditions for solid and liquid samples that can be levitated [27].

Frequency of sound in air	Maximum diameter of sample at 20 °C	Maximum diameter of sample at 400 °C
20 KHz	8.5 mm	13 mm
30 KHz	5.7 mm	8.6 mm
60 KHz	2.8 mm	4.3 mm

Table 1: Acoustic levitation conditions for solid samples

Liquid sample	Maximum diameter of sample	Maximum mass
Water (20 °C)	6.4 mm	0.14 g
Liquid tin (300 °C)	6.6 mm	1.05 g
Liquid tin (700 °C)	6.5 mm	0.98 g

Table 2: Acoustic levitation conditions for liquid samples

Standing wave levitation can easily be used to move and rotate objects in a three-dimensional space. Therefore, some of its applications include containerless processing of materials and handling systems [28].

3.4.2 Near-field acoustic levitation

NFAL occurs when the object being levitated acts as the reflector and a thin gas “squeeze film” is obtained between the source and the object. This film generates a time-averaged large levitation force. Objects are levitated within a short range, normally less than 1 mm. These characteristics make it possible to suspend or transport high-mass objects. Most near-field experiments have focused on the levitation of planar objects where both, the vibrating surface and the object’s reflecting surface, are planes.

Squeeze film levitation is suitable for guiding or transfer systems. It is limited to a two-dimensional movement [28].

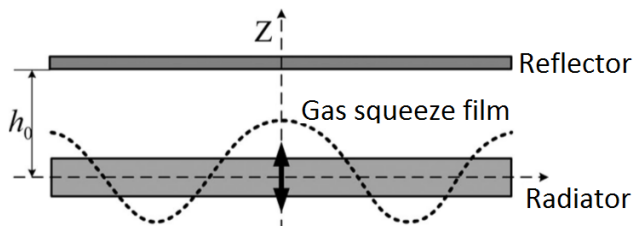


Figure 12: Near-field acoustic levitation [29]

3.4.3 Single-sided array levitation

Single-beam levitation uses a single-sided array that creates specific acoustic field patterns referred to as traps to maintain the floating object in place, while also focusing sound at a desired focal point.

As explained by Marzo [30], the array's phases can create these traps in the shape of tweezers, twisters, or bottles, considered the best mechanisms for containerless transportation. They are the result of variations in pressure and in the acoustic particle velocity.

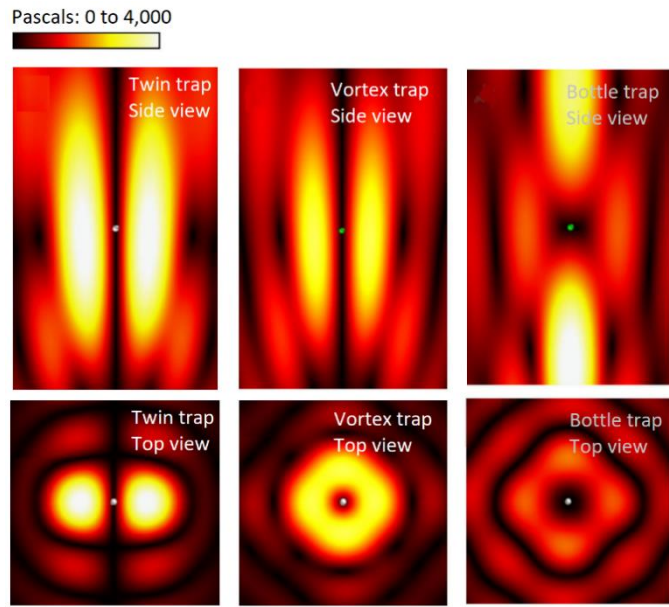


Figure 13 : Amplitude fields for three types of traps [30]

A twin trap is obtained by applying a π (or 180°) phase difference between the two halves of the phased array. A vortex trap is created by using a helicoidal pattern of phase difference. A bottle trap has a circular region of π -phase difference.

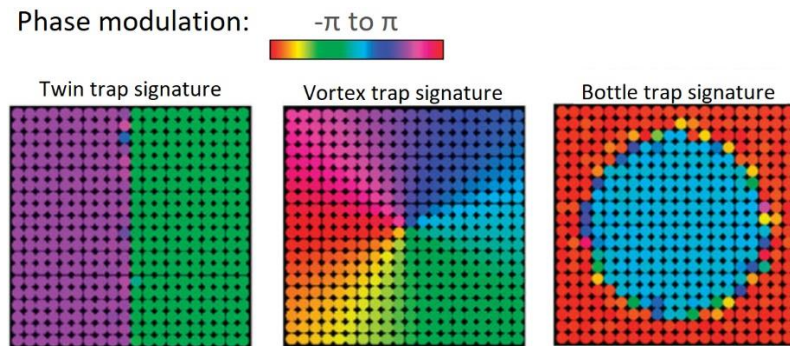


Figure 14: Phase signatures of acoustic traps [30]

3.4.4 Alternatives to levitation

The table below presents several techniques for object levitation and the advantages and disadvantages they have.

Levitation Technology	Advantages	Disadvantages
Magnetic	The levitation currents can rapidly adjust themselves when the suspended magnet is moved, turned, or put into oscillation. This allows for an almost instant levitation and keeping the object in suspension. This is because current in a superconductor has little resistance.	It is limited to materials with high electrical conductivity as well as low temperature applications. For electromagnetic systems, a feedback control loop is required to achieve an equilibrium position. The system is never completely stable in all degrees of freedom when only permanent magnets are used.
Electric	Several types of particles such as conductive, semi-conductive and dielectric materials can be manipulated. Large particles can be levitated.	Affected by temperature. Only low temperature fields have been proven to work. This is because at high temperature static charges cannot be maintained and they gradually degenerate as time passes by.
Optical	Long working distance.	Thermal forces make the levitation positions unstable. Optical tweezer techniques have been developed, but they lead to gripping forces that are very small and hardly reach 1 nN. Therefore, limited to very small particles.
Aerodynamic	Air flow is not affected by magnetism and it generates little heat. This is why pneumatic approaches can be applied to any material, including insulators, conductors, magnetic, non-magnetic, rigid and non-rigid.	Requires an external source of pressurized air which leads to poor lateral stability and a complex implementation. Poor energy efficiency, as only a small part of the mechanical energy of the pressurized air is used to move the object.
Ultrasonic	Acoustic standing wave levitators are capable of balancing objects that weigh a few grams. It is not necessary that the levitator is in an upright position. The levitator can be tilted or placed in a horizontal plane, and can serve as an acoustic microgripper. The angle between the axes of the sound transmitter and reflector can be up to 60°. This offers many gripping capabilities in micro-assembly. Any material, whether it be an insulator or a conductor, magnetic or non-magnetic, can be manipulated by acoustic forces. It is possible to achieve a stable equilibrium, as long as sufficient sound power is applied.	Acoustic streaming effect and non-uniformity of the force field. Streaming enhances heat and mass transfers. Asymmetries in the acoustic field result in undesired and uncontrolled sample rotations.

Table 3: Levitation technologies [28]

4. RESOURCES

4.1 Software

The table below presents the software used for the development of this project.

Software tool	Details
Xilinx Vivado Design Suite	<p>The Vivado Design Suite allows the creation of FPGA designs combining the ability of implementing them using an RTL to bitstream approach as well as including already-created intellectual property (IP) designs. These IP components can be selected from an IP catalog, and may be instantiated, configured, and interconnected with other modules using a block diagram approach. After the design is validated, it can be simulated, synthesized, and implemented. It is possible to estimate resource utilization, perform timing analysis and I/O planning before implementation [31].</p> <p>The hardware design and its bitstream file can be exported for its use in SDSoc.</p>
Xilinx SDSoc IDE	<p>The Software-Defined System On Chip environment allows the development of embedded systems in C/C++ using different SoC platforms, including the Zynq-7000 chip. The user can develop a software application and define a target platform. Some of the functions developed in software may be converted into hardware, to be implemented in programmable logic. It also permits importing a hardware design previously developed in Vivado [32].</p>
Ultraino Platform	This platform provides hardware, software, and example applications to control the transmission of narrowband airborne ultrasound.
Generic	Terminal emulator program for serial port communication.

Table 4: Software Resources

4.2 Hardware and Equipment

The table below presents the equipment used for the development of this project.

Hardware tool	Details
Avnet ZedBoard Kit	The ZedBoard is an evaluation and development board based on the Xilinx Zynq-7000 Extensible Processing Platform. It combines a dual Cortex-A9 Processing System with a Series-7 Programmable Logic section [33]. The programmable logic portion of the Zynq-7000 chip has arrays of CLBs to perform digital algorithms written in C or C++ or Register Transfer Level (RTL) code.
Ultrasonic Phased Array PCB Circuit	Details found in section 5.1.1.
DC Bench Power Supply	Single output DC bench power supply, 0-30V, 0-1A.
Polystyrene foam balls	Diameters used: 2.5 mm, 3 mm, 3.5 mm, 4 mm, 4.5 mm, and 5 mm.
Acoustically Transparent Mesh Fixture	Details found in section 5.2.1.

Table 5: Hardware Resources

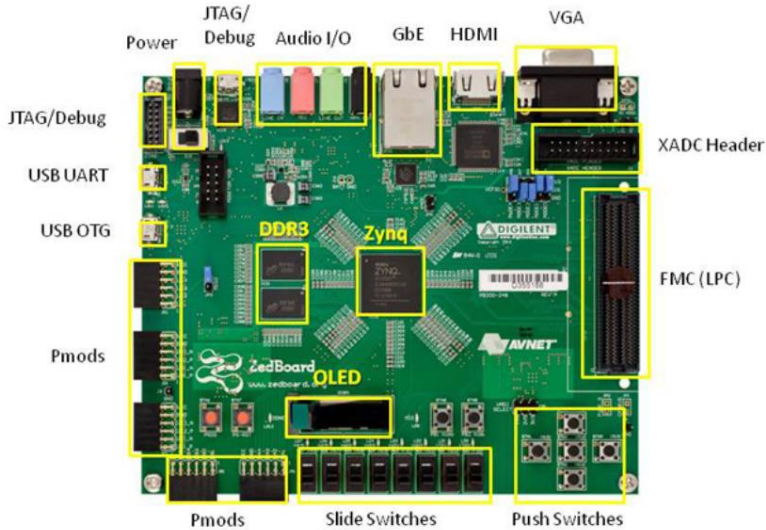


Figure 15: Zynq Evaluation and Development Board [34]

5. IMPLEMENTATION

5.1 Previous Work

This project is a continuation of previous work developed at the University of Bristol by William Beasley. The Zynq Evaluation and Development Board (ZedBoard) kit had been used to create an FPGA-based ultrasonic phased array driver which was capable of particle levitation using a standing wave levitation method. This board contains a Xilinx Zynq-7000 XC7Z020 chip that combines an ARM Cortex-A9 processing system with an FPGA fabric.

A PCB circuit containing MOSFET amplifier circuitry and an ultrasonic transducer array was also implemented. A reflector plate was fixed at a distance from the array to generate the required standing wave. Small polystyrene particles were successfully levitated below the nodes of the wave.

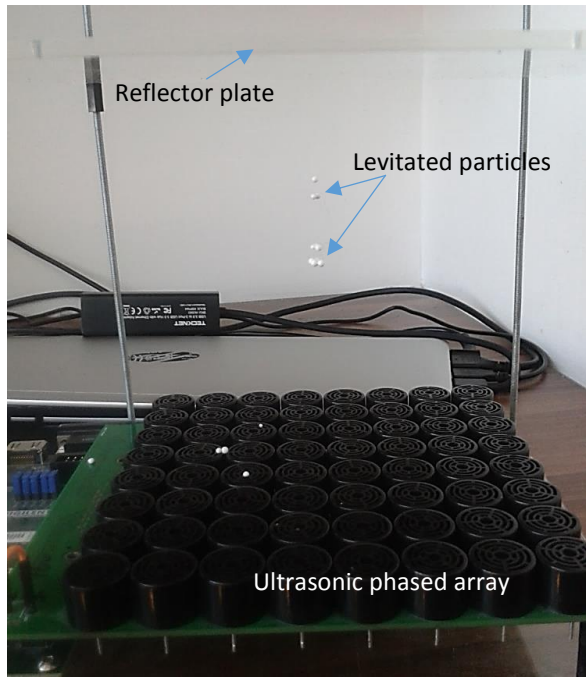


Figure 16: Previous setup using standing wave levitation

5.1.1 Ultrasonic Phased Array PCB Circuit

The primary side of the PCB circuit contains a squared-shape array of 64 MCUSD16P40B12RO ultrasonic transducers of 16.2 mm diameter each. An array of 32 dual-package TC4427A MOSFET drivers, located on the secondary side of the board, are used to amplify the output signals of an FPGA that drive the transducer elements, using 40 KHz, 16 V square wave signals. A Samtec FMC connector is used to interface the PCB circuit with the FPGA.

The figure below presents a coordinate map of the phased array, where the origin is located on the top left corner. The transducers are numbered from 0 to 63, starting from the top left and counting downwards.

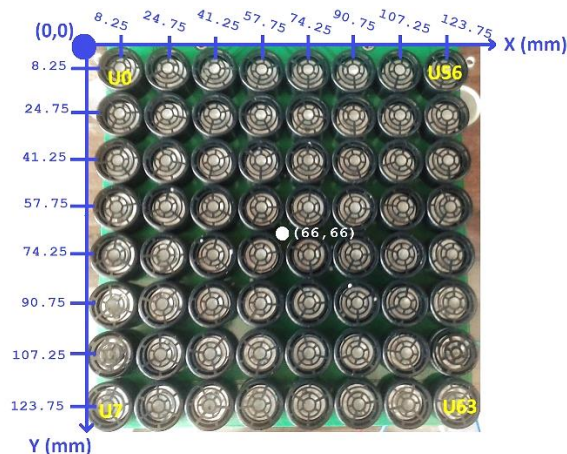


Figure 17: Coordinates on phased array

5.1.2 System Design

The system was developed in Xilinx Vivado using the Zynq-7000 SoC platform. The design incorporates an ARM Cortex-A9 processing system that communicates with an ultrasonic phased array driver module via an AXI Interconnect IP hardware component, in a master-slave manner. The software of the processing system has been developed in C language. The ultrasonic phased array driver was directly developed in VHDL code.

To achieve levitation the processor requires the 3-D coordinates in millimetres (X, Y, and Z) where the desired focal point will be placed. These coordinates are used to calculate the distance from each element of the array to the focal point. The distance is divided by the sound wavelength. The remainder of this division is expressed as a fraction of the sound's wavelength. Multiplying this number by 2π corresponds to a phase shift value, which is used to delay a zero-phase shifted 40 KHz square wave signal. A total of 64 phase shift values are converted into 8-bit numbers that are ordered in a total of 16 32-bit words, each word containing 4 phase shift values. A Match array organizes all 16 words to be communicated to the ultrasonic driver module via the AXI interconnect.

The ultrasonic driver module has an 8-bit counter module, which increments its value every 97.65 ns, using a 10.24 MHz clock. After counting from 0 to 255, a 25 us period will have passed. This period corresponds to a 40 KHz frequency.

A 256-bit logic vector has been defined and hardcoded with bits 0 to 127 populated with '1's and bits 128 to 255 populated with '0's. The 8-bit counter is used to iterate through this logic vector, to create one period of a zero-phase shifted square wave signal.

The ultrasonic module also includes a total of 64 submodules that create the required 40 KHz phase shifted signals to drive the transducer elements. Each submodule uses the zero-phase shifted signal as an input, the 8-bit counter, and the corresponding phase shift value previously calculated by the processing system.

With every rising edge of the clock, each submodule subtracts the count value of the 8-bit counter minus the 8-bit phase shift value. The result is used as an index to one of the bits of the 256-bit logic vector. The indexed bit is then output to drive the MOSFET amplifier.

5.1.3 Focal Point Width

The width of the focal point for this 8x8 transducer array can be calculated using a focal length R of 100 mm, a distance D equivalent to the transducer element diameter of 16.2 mm by a total of 8 elements per side, and speed of sound equal to 340.29 m/s at a temperature of 15°C, as follows:

$$w = 2\lambda \frac{R}{D} = 2\left(\frac{c}{f}\right) \frac{R}{D}$$
$$w = 2\left(\frac{340.29 \text{ m/s}}{40 \text{ KHz}}\right) \frac{0.1 \text{ m}}{(0.0162\text{m})(8 \text{ transducers})} = 13.12 \text{ mm}$$

Equation 8: Focal point width for the phased array used

5.2 Current Work

This project uses the same ultrasonic phased array driver and previously coded C functions of the processing system that are used to calculate the phase shift values, as well as PCB circuit.

It builds on the previous work described by enhancing the design to achieve single-sided beam mid-air levitation. This type of levitation is different from the standing wave method, as it does not require a reflector plate to suspend a particle. The new design also incorporates an echo reception feature as a form of feedback to the system, making the design responsive to external stimulus.

A stable levitation is achieved by adding a temperature sensor to correct the speed of sound value and its wavelength. A user interface has been incorporated to demonstrate movement of a levitated particle along the XY-plane of the array.

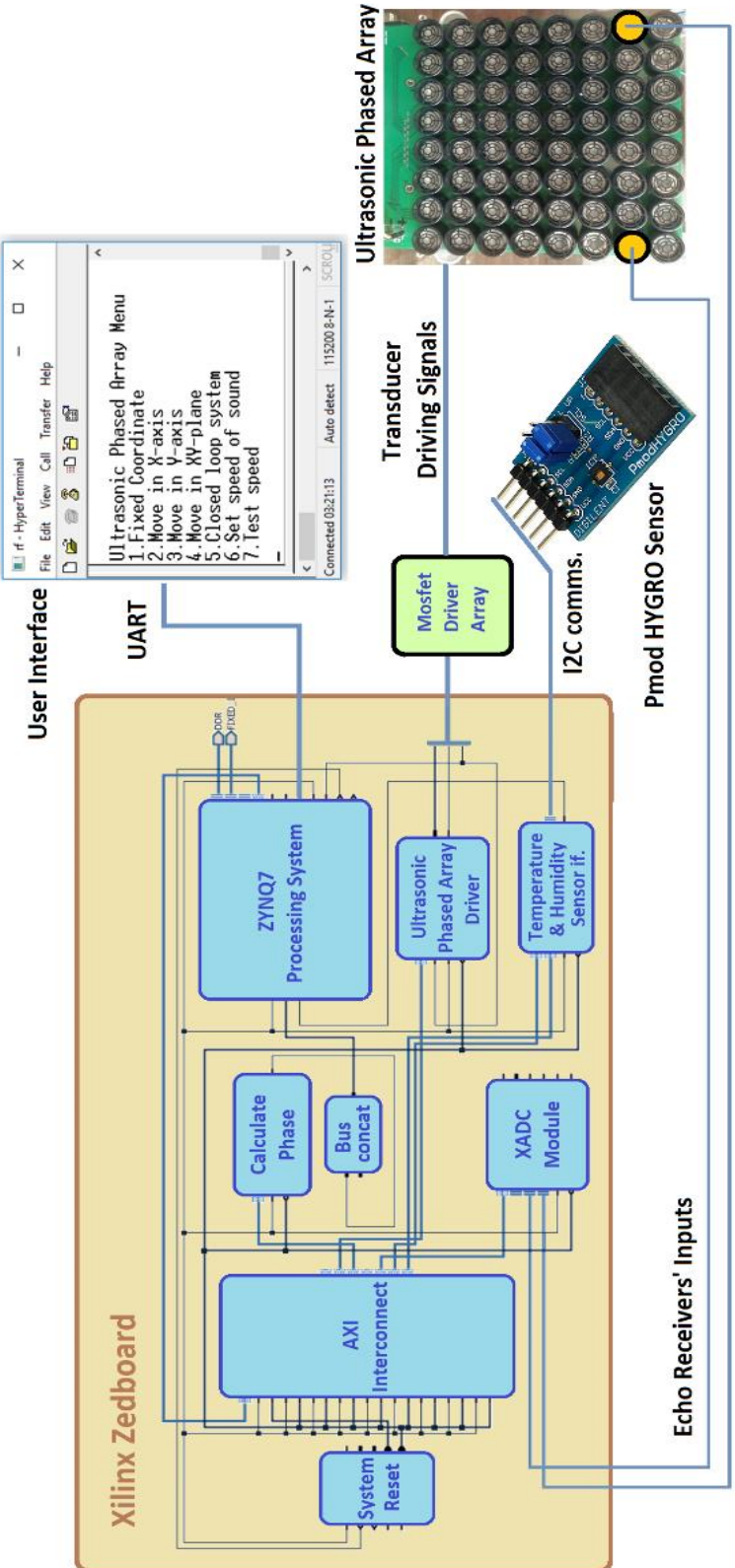


Figure 18: System block diagram

The design structure of the full system implemented in Xilinx Vivado is shown below.

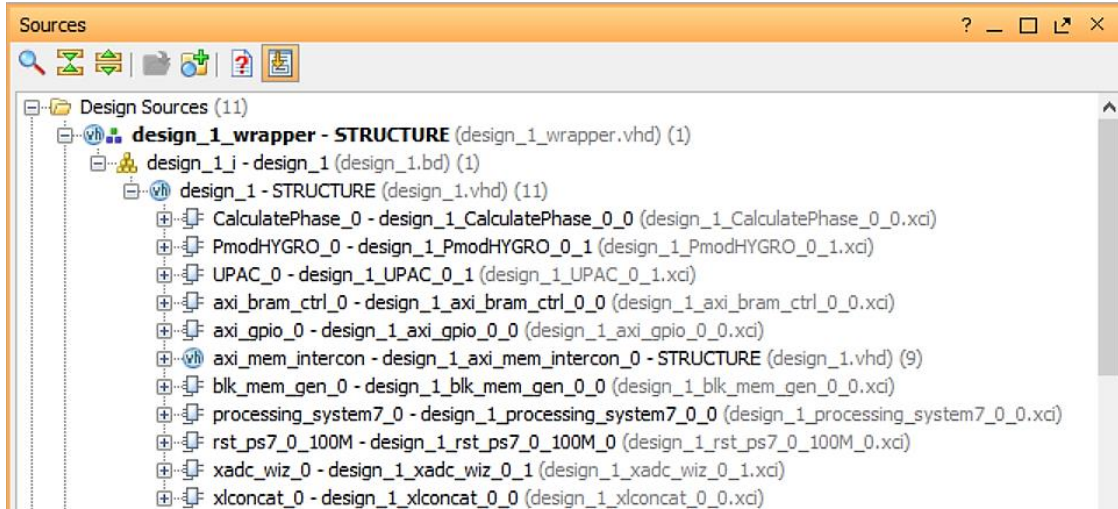


Figure 19: Vivado system structure

The following sections present the consecutive steps that were carried out for the implementation of this project.

5.2.1 Acoustically Transparent Mesh Fixture

An acoustically transparent mesh allows sound waves to travel through without interference or reflections. A fixture using a 200 mm X 300 mm and 0.2 mm thick mesh of this kind was built, fixing the mesh with four 200 mm-long screws that permitted adjusting its height. The mesh was attached to a metal frame to ensure a flat and rigid surface. The height of the mesh was set at approximately 100 mm, corresponding to the focal length R .



Figure 20: Acoustically transparent mesh fixture side and top views

As a first step towards single-beam levitation, the fixture was used to examine whether small polystyrene foam spheres ranging between 2 and 5 mm could be moved from one position to another, having only the support of the mesh, without the presence of a standing wave. The original SoC design described under section 5.1.2 was used for real time generation of

focal points. The focal point was fixed at coordinates (66,66,100), corresponding to the center of the phased array.

It was found that placing a particle in the position of the focal point would cause it to roll to the side or be ejected away from the acoustic beam. It was not possible to maintain the object in the focal point's position.

5.2.2 Twin-Trap Creation

5.2.2.1 Simulation in Ultraino platform

To overcome particle ejection, an acoustic trapping mechanism, as described in section 3.4.3, was utilized. A twin-trap was selected, as this is the easiest to create and include within the phase shift calculations for each transducer element. This trap requires a π -phase difference of the transducers' square wave signals between both halves of the phased array.

To verify that the 8x8 phased array being used would be able to generate the twin-trap acoustic field with enough strength, it was first simulated using the Ultraino platform, developed at the University of Bristol. This platform provides hardware, software, and example applications to control the transmission of narrowband airborne ultrasound. The software uses Java 1.8 to support a multiplatform environment, as well as OpenGL for 3D graphics creation, and GLSL 3.0 to plot the acoustic fields [35].

The software permits defining the geometry of the array and a predefined beamforming operation. This includes focusing or generating a trap at a specific point in space. It also calculates both the amplitude and phase of the acoustic field emitted by the array, as well as the acoustic radiation forces [35].

The acoustic field amplitude and phase were modelled as shown in Figures 21 and 22 for the square 8x8 phased array used (64 elements), in which each MCUSD16P40B12RO transducer operates at 40 KHz and has a 16.2 mm diameter,

Amplitude: 0 to 1500 Pa

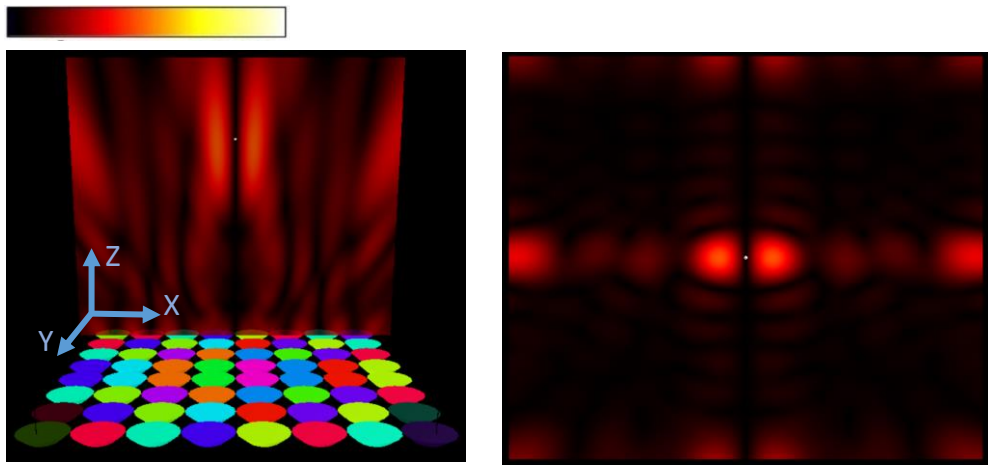


Figure 21: Side and top views of twin trap amplitude field

Phase: $-\pi$ to π

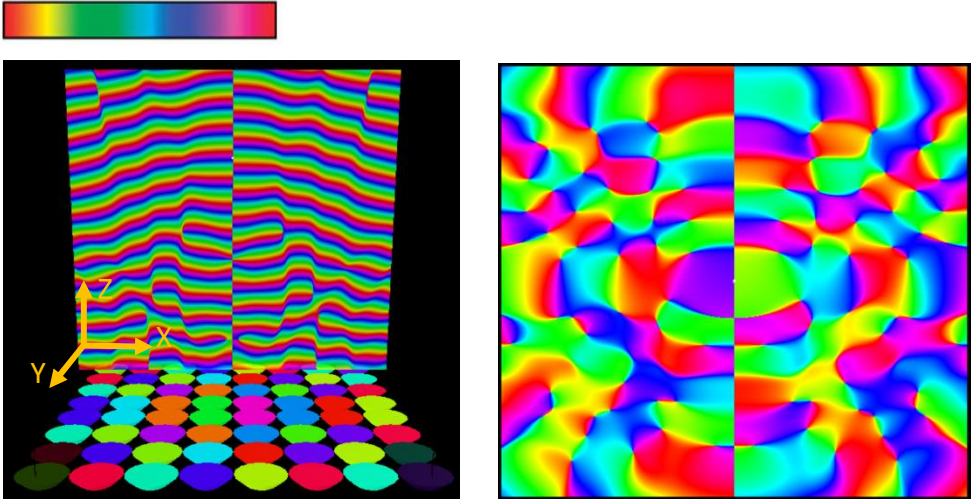


Figure 22: Side and top views of twin trap phase field [35]

The lateral and longitudinal forces exerted on a 1 mm diameter polystyrene sphere contained in the center of the phased array using an ultrasound frequency of 40 KHz were also simulated. These forces converge in the coordinates origin.

Considering the center of the twin-trap at the origin, the arrows along X and Y, shown in the figures below, represent the direction of the lateral radiation force vectors that hold the particle in place, pushing it towards the middle of the trap. In the case of the longitudinal force along the Z axis, the yellow arrow represents a positive force that pushes the particle upwards.

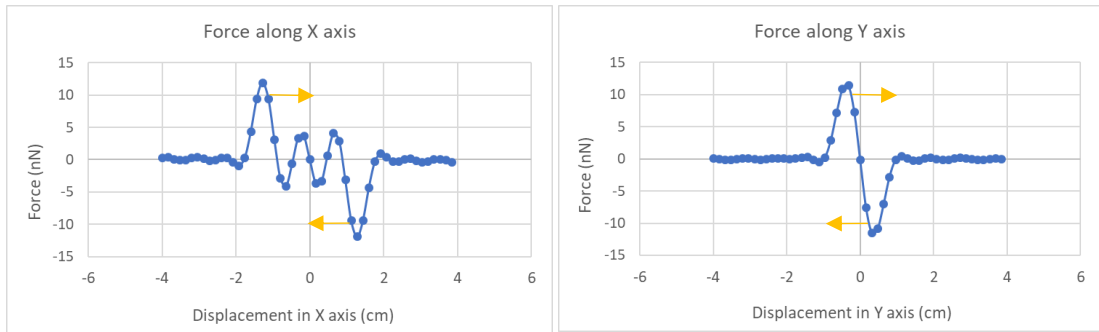


Figure 23: Acoustic twin-trap lateral forces

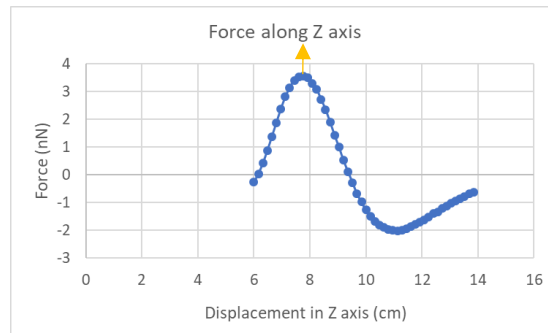


Figure 24: Acoustic twin-trap longitudinal force

5.2.2.2 Twin-Trap Implementation in C application

The twin-trap previously simulated was implemented in embedded C language as part of the phase shift calculation performed by the Zynq-7000 processing system. Considering a 64-element square array, since the phase shift can be expressed in units of fraction of a wavelength, that is between 0 and 1, it is necessary to add 0.5 of a wavelength to the individual phase shift values of transducers U32 to U63, while maintaining the phase shift values as they are for transducers U0 to U31.

The final phase shift calculation is expressed as the individual phase shift, which depends on the position of the transducer element with respect to the focal point, plus the twin-trap additional shift. The sum is multiplied by 2π . If the result is greater than 2π , i.e. greater than one wavelength, it is necessary to adjust the result by subtracting 2π :

For elements U0 to U31:

$$\phi_i = 2\pi \left(\frac{\text{mod} \left(\frac{L}{\lambda} \right)}{\lambda} \right)$$

Equation 9: Phase shift calculation for transducers U0 to U31

For elements U32 to U63:

$$\phi_i = 2\pi \left(\frac{\text{mod} \left(\frac{L}{\lambda} \right)}{\lambda} + 0.5 \right)$$

Equation 10: Phase shift calculation for transducers U32 to U63

where ϕ_i is the phase shift in radians, L is the distance between the transducer and the focal point, and λ is the sound's wavelength.

5.2.3 Echo wave capture

Echo wave reception was enabled as a form of feedback to the system. The two main purposes of feedback included the estimation of the levitated particle's position and the response of the system to the presence of objects other than the particle.

Feedback was introduced by modifying the SoC design previously implemented in Xilinx Vivado, as well as adapting the PCB, containing the MOSFET amplifiers and phased array.

5.2.3.1 XADC core in Vivado design

A Xilinx AXI XADC core was incorporated into the Zynq-7000 programmable logic of the SoC design. Its purpose was to monitor two phased array transducer inputs, acting as echo receivers. The XADC core is a 32-bit slave peripheral with an AXI4-Lite interface that can monitor internal on-chip supply voltages and temperature, as well as having one dedicated analog input pair and 16 auxiliary differential analog input pairs, with conversion rate of 1 MSPS. It can measure unipolar or bipolar measurements, and allows for a maximum signal bandwidth of 500 KHz for the dedicated input pair, and 250 KHz for the auxiliary inputs [36].

For this application, the Xilinx XADC Wizard was used to generate an HDL wrapper of the ADC module. It was configured to work in Continuous Mode, using a Channel Sequencer, and enabling bipolar auxiliary inputs Vaux4 and Vaux10.

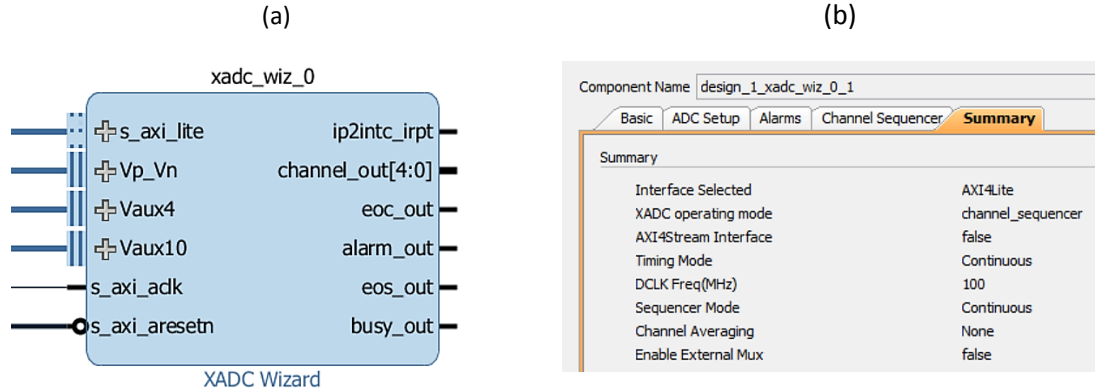


Figure 25: AXI XADC core (a) and XADC configuration (b)

One of the reasons for selecting these two inputs was to be able to reuse and modify the available PCB circuit, in which the FPGA's outputs located on the FMC port of the Zedboard had already been routed to the MOSFET chips driving specific transducer elements, but could also be configured as XADC inputs.

A second reason for selecting them was that they were positioned symmetrically on the edges of the array. Additionally, it was observed that choosing more centric transducers in the array would have reduced the strength of the acoustic radiation which permits levitation. This implies a tradeoff between levitation capability and echo reception, where levitation has a higher priority.

These auxiliary input pairs are found on Bank 35 of the Zynq-7000 chip. The Vaux4 pair is routed to the Zedboard's FMC J1A port at LA18_P and LA18_N. The Vaux10 pair is routed to the Zedboard's FMC J1B port at LA31_P and LA31_N.

A detailed explanation of the PCB modification is found in section 5.2.3.3.

The XADC component was connected to the AXI Interconnect IP module which manages the interaction between the slave modules and the processing system.

5.2.3.2 Enabling the XADC module in the SDx Environment

The updated hardware design was exported from Vivado as a hardware description file (.hdf) into the SDx environment, where the embedded C application project used by the processing system is found. The .hdf file contains the drivers and bitstream file to program the FPGA.

(a) (b)

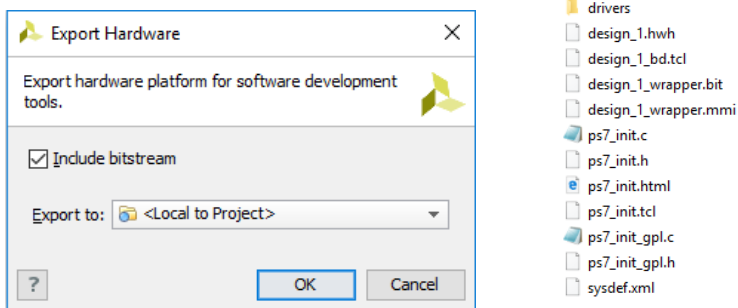


Figure 26: Exporting the hardware platform (a). Content of .hdI file (b)

Within the C application, the XADC component was initialized and a GetEchoData() function created to acquire a 400-sample echo from each of the two receiver inputs, Vaux4 and Vaux10.

5.2.3.3 PCB modifications for echo reception

The PCB circuit containing the 32 dual-package MOSFET TC4427A driver array and the 64 Multicomp MCUSD16P40B12RO ultrasonic transducers was modified to enable the reception of echo acoustic waves. Two transmitters, U6 and U62, located at positions (8.25, 107.25) and (123.75, 107.25) were converted to receivers. This was achieved by removing their MOSFET amplifiers and connecting a $100\ \Omega$ resistor between the ends of each transducer and their respective tracks routed to the FMC connector.



Figure 27: PCB modifications

Since transmitters U7 and U63 originally shared their MOSFET driver dual-package with U6 and U62 respectively, they became disabled with this modification and were no longer able to transmit acoustic signals.

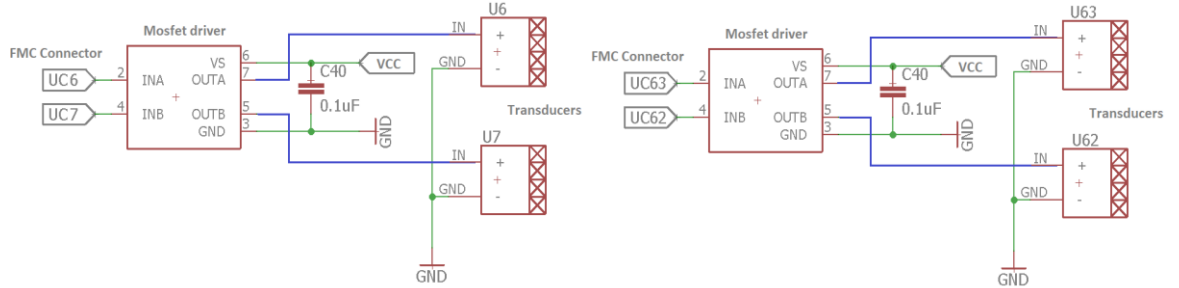


Figure 28: Original circuit

In the figure below, UC6 and UC7 FPGA outputs acting as driving signals for U6 and U7 transducers were converted to differential ADC inputs for U6. The same modification was applied to U62 and U63.

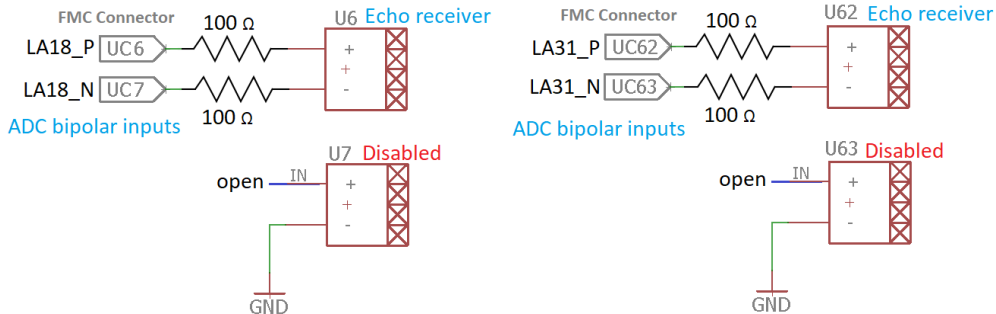


Figure 29: Modified circuit

With the purpose of obtaining better echo reception, the receivers were lifted and inclined towards the center of the array.



Figure 30: Receiver inclined position

5.2.4 Speed of sound adjustment for temperature variation

During the process of testing for single-beam levitation of a particle, it was observed that the particle's stability and ability to levitate in mid-air were significantly affected by the characteristics of the environment, mainly temperature variations. It was found that the speed of sound increases with temperature. Its rate of change can be approximated to the linear function below:

$$c \approx 331.3 + 0.6(\text{Temperature } ^\circ\text{C}) \text{ m/s}$$

Equation 11: Speed of sound with temperature variations [37]

If the speed of sound increases, the wavelength of sound becomes larger with temperature, as well. Considering the wavelength value is used to calculate the phase shifts of the 40 KHz driving signals, this means that the phase shifts are also affected. Since the wavelength is also used to determine the width of the focal point by $w = 2\lambda \frac{R}{D}$, this measurement will also change approximately in a linear manner.

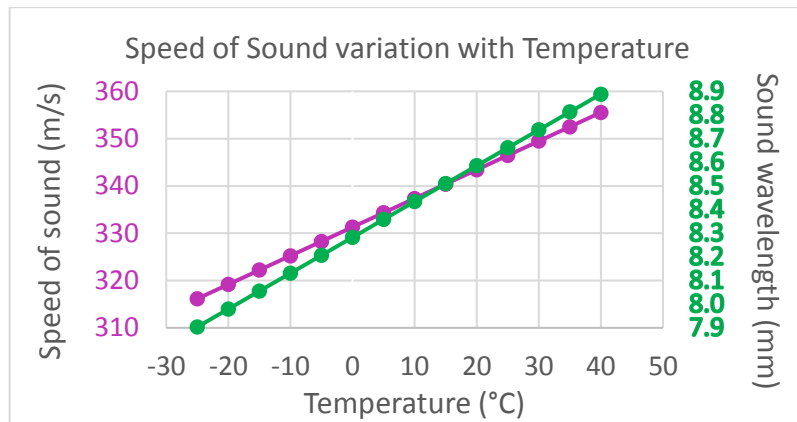


Figure 31: Speed and wavelength of sound with temperature

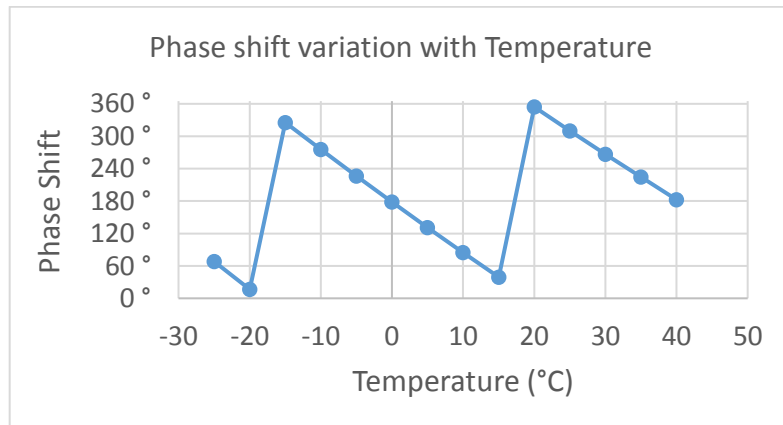


Figure 32: Phase shift variation with temperature

The following graph shows the focal point width variation for the 8x8 phased array used, where the focal length R is 100 mm.

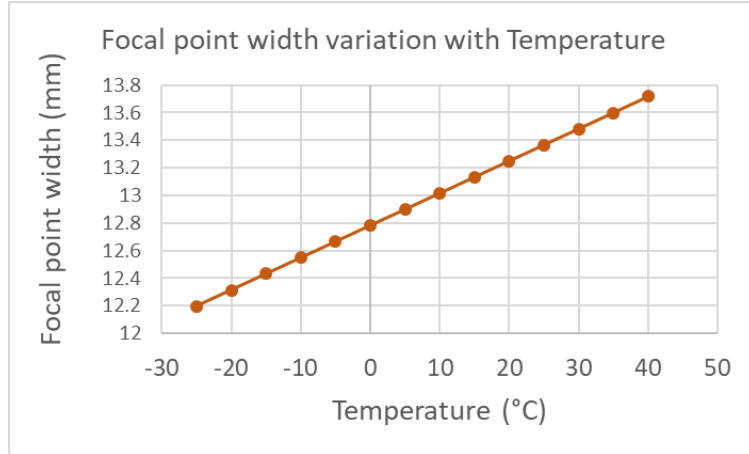


Figure 33: Focal point width variation with temperature

To compensate for temperature variations affecting the speed of sound, a Pmod HYGRO sensor was added to the system. This sensor can digitally report the relative humidity and ambient temperature upon request by the host board with up to 14 bits of resolution. It provides a relative humidity accuracy of $\pm 2\%$ and a temperature accuracy of $\pm 0.2^\circ\text{C}$. Communication with this board is performed via a 6-pin Pmod connector with I²C interface [38].

The Pmod HYGRO sensor driver was downloaded from the Digilent Vivado library, which contains several Pmod IP cores and interfaces that are compatible with the Xilinx Vivado IP Catalog. The directory was included as a repository within the Vivado design.

Within the Vivado design, the Pmod HYGRO IP component was added and connected to the AXI Interconnect module, to provide temperature measurements to the processing system. An I²C interrupt line was wired from the Pmod HYGRO core to an IRQ input of the processor.

The processing system reads a temperature measurement when requested by the user, and updates the speed of sound value and its wavelength.

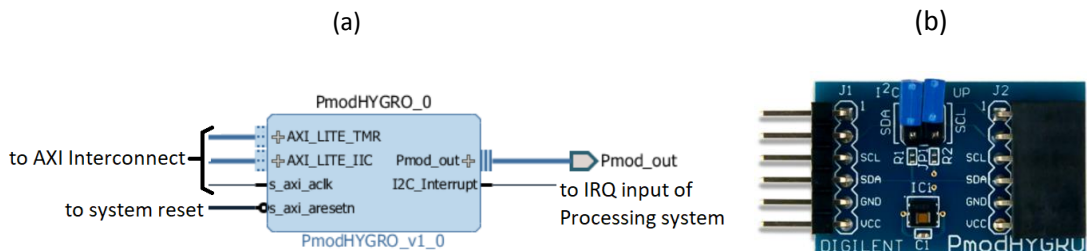


Figure 34: Pmod HYGRO sensor IP component (a) and sensor PCB (b) [38]

5.2.5 Embedded C application in SDx environment

The embedded C application runs on the Zynq-7000 processing system. The program first initializes the hardware IP components implemented in the programming logic of the chip. These include the XADC module, the Ultrasonic Phased Array Driver, the Pmod HYGRO Sensor and the UART interface for serial port communication.

It then provides a list of options for driving the ultrasonic phased array. After the user selects an option via the serial port interface, it creates the desired focal points along the XY plane, maintaining a constant focal length of 100 mm.

If echo reception is enabled, in order to properly listen to any echoes returning to the phased array, the transducer elements are momentarily disabled for a period of 3.8 ms. Once the system is in a quiet state, the transducers are enabled for only 300 us to create a small burst of acoustic waves that arrive to the focal point and may be reflected from the levitated particle. The transducers are disabled again afterwards, while the ADC samples are read to capture possible echoes.

The XADC module captures a 400-sample waveform for each of the two receiver channels, Vaux4 and Vaux10. The peak amplitude values and the ADC sample number at which they occur are recorded. They are used to estimate the position of the particle and to react if a threshold voltage of 110 mV is surpassed.

The user interface options and particle position estimation are described in the sections below.

5.2.5.1 UART user interface

A user interface was included in the embedded C application of the Zynq-7000 processing system, establishing communication between the Zedboard and a PC station. It was created to demonstrate the ability of the system to levitate a small polystyrene particle. The system presents the options listed in Figure 35(a). A serial port session is used to establish communication with the system, using the port settings shown in Figure 35(b).

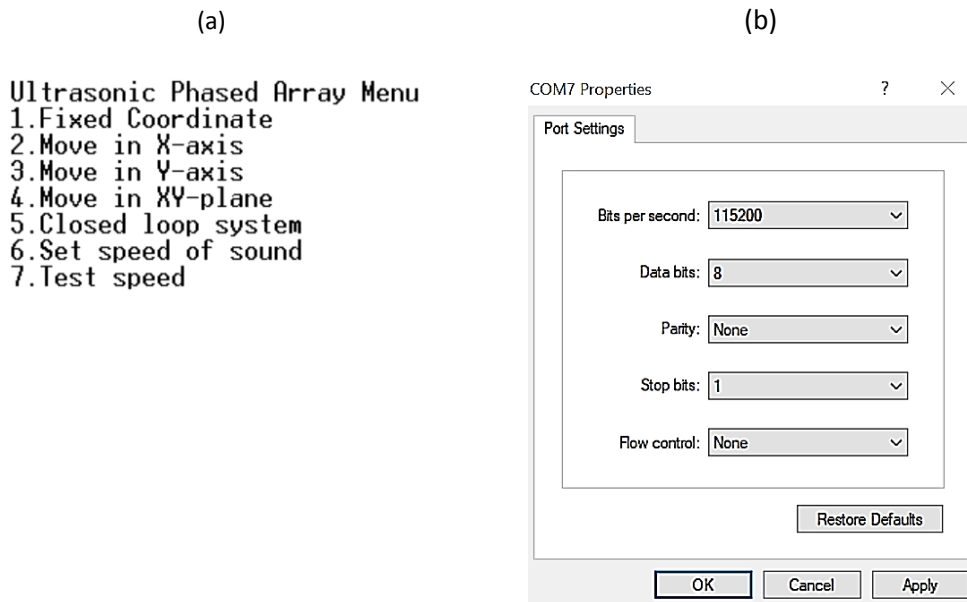


Figure 35: User interface menu (a). UART interface configuration (b)

1) Fixed Coordinate

This option requests the focal point coordinates X and Y within a range of 50 to 70 mm, using a focal length of 100 mm. It creates a static focal point on the coordinates selected.

```
Selected: 1
Requested X-coordinate (between 50 and 70):
Requested Y-coordinate (between 50 and 70):
Coordinates: (61,65,100)
```

Figure 36: User interface - Fixed coordinate option

2) Move in X-axis

This option moves the particle in the X axis within the range of 63 to 69, using a 1 mm step size, and keeping the Y axis constant. Focal length is set to 100 mm.

It allows the user to enable or disable echo reception. When feedback is enabled, the system tries to guess the X coordinate based on statistical measurements. If it is not able to distinguish the coordinate, it reports it as *Undefined*.

```
Selected: 2
Enable feedback? (y/n)
Echo enabled
Press any key to return to this menu
CurrentX: 63 Guessed options: 63,64,65,69 count4: 159 count10: 151
CurrentX: 64 Guessed options: 64,67,68,69 count4: 171 count10: 150
CurrentX: 65 Guessed options: 67,68,69 count4: 168 count10: 160
CurrentX: 66 Guessed options: Undefined count4: 199 count10: 199
```

Figure 37: User interface – Move in X-axis

3) Move in Y-axis

This option moves the particle in the Y axis within the range of 63 to 69, using a 1 mm step size, and keeping the X axis constant. It does not have an echo reception option enabled. Focal length is set to 100 mm.

4) Move along XY plane

This option moves the particle in the XY plane in a serpentine pattern, from coordinates (63,63) to coordinates (69,69), using a focal length of 100 mm. The particle is then moved back to its starting point. It does not have an echo reception option enabled.

5) Closed Loop System

This option places the particle in a fixed point. It then enables echo reception and sets a voltage threshold of 110 mV. If receiver Vaux4 captures an echo with a maximum amplitude higher than the threshold, the particle is moved to the right along the X-axis, until it reaches coordinates (69,66). If the echo captured by receiver Vaux10 rises above threshold, the particle is moved to the left until it reaches coordinates (63,66). If both echoes captured are higher than the threshold, the particle is moved in opposite direction of the receiver with higher amplitude.

```
Selected: 5
Press any key to return to this menu
CurrentX: 63 count4: 160 count10: 151 peak4: 0.026 peak10: 0.062
CurrentX: 63 count4: 175 count10: 160 peak4: 0.019 peak10: 0.086
CurrentX: 63 count4: 153 count10: 186 peak4: 0.500 peak10: 0.117
CurrentX: 69 count4: 185 count10: 153 peak4: 0.048 peak10: 0.056
CurrentX: 69 count4: 188 count10: 156 peak4: 0.044 peak10: 0.074
CurrentX: 69 count4: 188 count10: 181 peak4: 0.038 peak10: 0.236
CurrentX: 63 count4: 175 count10: 166 peak4: 0.032 peak10: 0.094
```

Figure 38: User interface – Closed Loop System

6) Setting speed of sound

This option reports temperature and relative humidity of the environment. It uses the temperature measurement to correct the speed of sound and wavelength values used for the phase shift calculations of the 40 KHz driving signals.

```
Selected: 6
1.Default speed of sound
2.Adjust to temperature
Temperature: 21.74 degC Humidity: 61.74 RH
Speed of sound: 344.342957 Wavelength: 0.008609
```

Figure 39: User interface – Setting speed of sound and wavelength

7) Testing the speed of a particle

This option requests a step size in millimeters and a delay factor. It then moves the particle along the X axis with the values provided and reports the speed achieved in mm/s. This test was used to determine the maximum average speed achieved by a 4 mm particle for a specific step size.

```
Selected: 7
Set step (mm):
Set delay factor (50 to 8000):
Step: 1.000000 Delay: 300
Step: 1.000  Delay: 300 Speed: 2.240 mm/s Time: 8036092 us
Step: 1.000  Delay: 300 Speed: 2.237 mm/s Time: 8047765 us
```

Figure 40: User interface – Test speed of particle

5.2.5.2 Particle Position Estimation

Two methods for estimating the position of the levitated particle were evaluated: a geometrical approach and a statistical analysis.

Geometrical method:

This method uses Pythagoras theorem to determine the unknown coordinates X and Y where the levitated particle should be. The Z plane is kept constant and is a known value equal to the focal length, 100 mm.

If the speed of sound and the time of arrival of an echo to receivers Vaux4 and Vaux10 is known, it is possible to determine the total distance that each echo had to travel from its origin, located at the transmitter. The total distance is then divided by 2 to obtain the distance from the particle's position to the receivers, $d_{particle-RX}$.

The coordinates of both receivers are:

- Vaux4 receiver: (8.25,107.25,12)
- Vaux10 receiver: (123.75,107.25,12)

The distance between the particle and each echo receiver is:

$$d_{particle-Vaux4} = \sqrt{(X - 8.25)^2 + (Y - 107.25)^2 + (100 - 12)^2}$$

$$d_{particle-Vaux10} = \sqrt{(X - 123.75)^2 + (Y - 107.25)^2 + (100 - 12)^2}$$

Equation 12: Distances between the particle and each echo receiver

These two equations can be expressed as follows:

$$X^2 - 247.5X + 15314.06 + Y^2 - 214.5Y + 19246.6 - d_{particle-Vaux4}^2 = 0$$

$$X^2 - 16.5X + 68.06 + Y^2 - 214.5Y + 19246.6 - d_{particle-Vaux10}^2 = 0$$

Since both equations share common terms:

$$-247.5X + 15314.06 - d_{particle-Vaux4}^2 = -16.5X + 68.06 - d_{particle-Vaux10}^2$$

Solving for X and Y:

$$X = \frac{15246 + d_{particle-Vaux4}^2 - d_{particle-Vaux10}^2}{231}$$

$$Y = \frac{214.5 - \sqrt{4(d_{particle-Vaux4}^2) - 4X^2 + 66X - 40272.25}}{2}$$

Equation 13: Calculation of X and Y coordinates with geometrical method

This approach was not used as the time of arrival of the echoes was difficult to discern from the captured waveforms. Due to the limited number of receivers on the array there were cases when no echo was detected.

Statistical Analysis

For this approach, the levitated particle was moved along the X-axis, from coordinates (63,66,100) to (69,66,100), keeping Y and Z constant. The echoes were captured for a total of 7 coordinates, and the ADC sample numbers at which their peak amplitudes occurred were recorded. This process was repeated 50 times to obtain statistical measurements to correlate each coordinate with the sample number of the peak value.

This method was used to estimate particle position within *Option 2: Move in X-axis* with echo reception enabled. The software reports the coordinates of the focal point and the guessed coordinates for comparison.

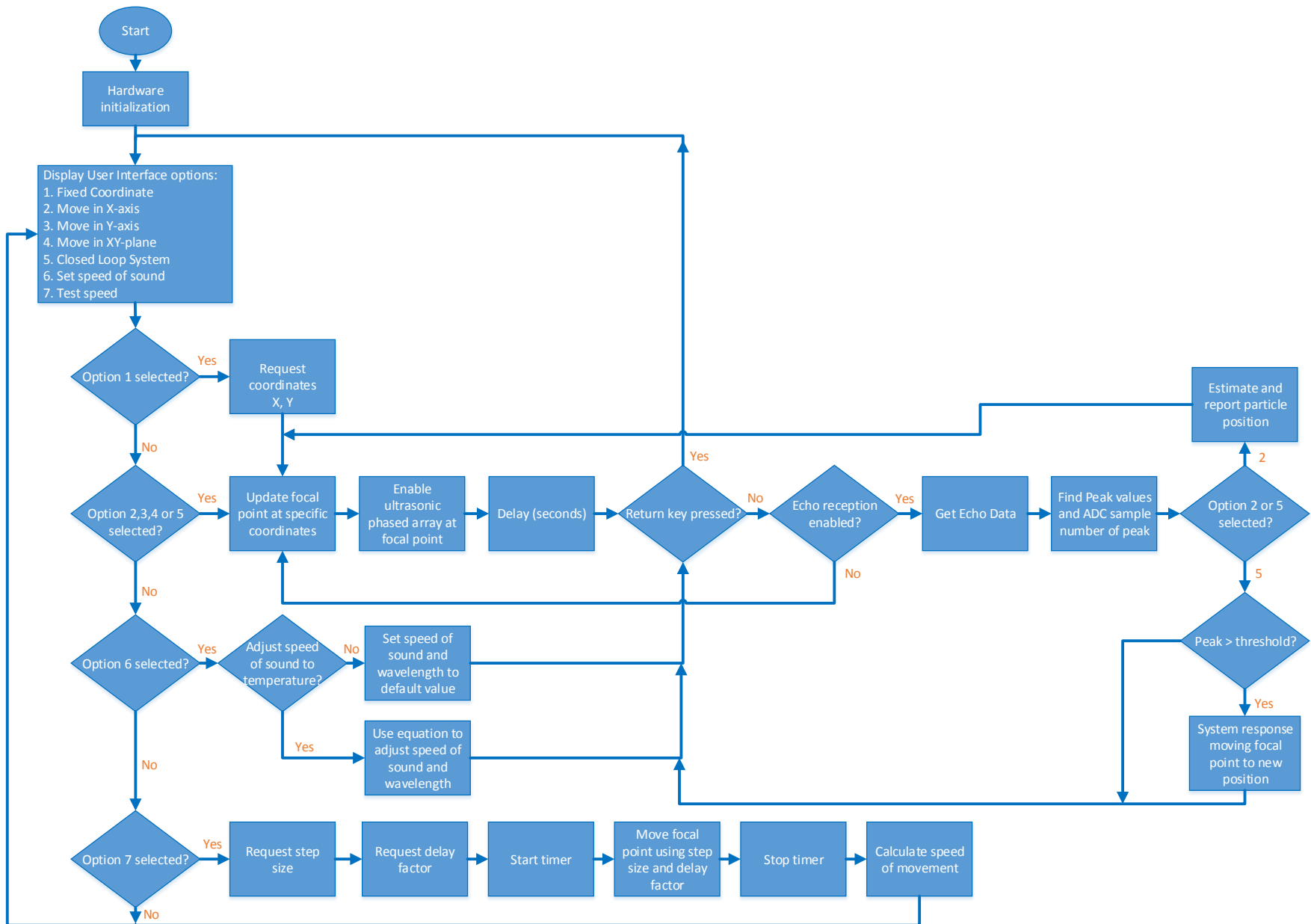


Figure 41: Flow diagram of embedded C software application

6. RESULTS

6.1 Implemented Design Details

6.1.1 FPGA Resources Utilization

The following figures present a summary of the hardware design resources utilization.

Site Type	Used	Fixed	Available	Util%
Slice LUTs	7841	0	53200	14.74
LUT as Logic	7374	0	53200	13.86
LUT as Memory	467	0	17400	2.68
LUT as Distributed RAM	0	0		
LUT as Shift Register	467	0		
Slice Registers	9089	0	106400	8.54
Register as Flip Flop	9089	0	106400	8.54
Register as Latch	0	0	106400	0.00
F7 Muxes	129	0	26600	0.48
F8 Muxes	0	0	13300	0.00

Site Type	Used	Fixed	Available	Util%
Block RAM Tile	2	0	140	1.43
RAMB36/FIFO*	2	0	140	1.43
RAMB36E1 only	2			
RAMB18	0	0	280	0.00

Site Type	Used	Fixed	Available	Util%
DSPs	10	0	220	4.55
DSP48E1 only	10			

Figure 42: Programmable Logic resource utilization

6.1.2 FPGA Timing Summary

The timing summary of the implemented design is presented below.

Setup	Hold	Pulse Width
Worst Negative Slack (WNS): 0.214 ns	Worst Hold Slack (WHS): 0.019 ns	Worst Pulse Width Slack (WPWS): 4.020 ns
Total Negative Slack (TNS): 0.000 ns	Total Hold Slack (THS): 0.000 ns	Total Pulse Width Negative Slack (TPWS): 0.000 ns
Number of Failing Endpoints: 0	Number of Failing Endpoints: 0	Number of Failing Endpoints: 0
Total Number of Endpoints: 18357	Total Number of Endpoints: 18357	Total Number of Endpoints: 9601

All user specified timing constraints are met.

Figure 43: Design Timing Summary

6.1.3 FPGA Power Consumption

A power consumption summary of the hardware implementation is presented below.

Total On-Chip Power (W)	1.800	
Dynamic (W)	1.640	
Device Static (W)	0.160	
Effective TJA (C/W)	11.5	
Max Ambient (C)	64.2	
Junction Temperature (C)	45.8	
Confidence Level	Low	
Setting File	---	
Simulation Activity File	---	
Design Nets Matched	NA	

Figure 44: FPGA Power Report Summary

On-Chip	Power (W)	Used	Available	Utilization (%)
Clocks	0.032	4	---	---
Slice Logic	0.031	20688	---	---
LUT as Logic	0.026	7374	53200	13.86
CARRY4	0.003	693	13300	5.21
Register	0.002	9089	106400	8.54
LUT as Shift Register	<0.001	467	17400	2.68
F7/F8 Muxes	<0.001	129	53200	0.24
Others	0.000	1436	---	---
Signals	0.037	14706	---	---
Block RAM	0.002	2	140	1.43
DSPs	0.005	10	220	4.55
I/O	0.002	91	200	45.50
XADC	0.002	1	---	---
PS7	1.529	1	---	---
Static Power	0.160	1	1	1
Total	1.800	1	1	1

Figure 45: On-Chip component power consumption

6.1.4 Phased Array Power Consumption

The total power consumption of the ultrasonic phased array was estimated to be 2.64 W. The maximum constant voltage of 16.5 V and current of 160 mA were used to enable particle levitation.

6.2 Achieving Mid-Air Levitation

The twin-trap mechanism was tested using the acoustically transparent mesh fixture for support. It was observed that the size and shape of the object significantly affect its levitation capability as well as its stability if capable of levitating at all. Using a static focal point at a height of 100 mm from the phased array, some polystyrene foam spheres would achieve levitation for a few seconds, before becoming unbalanced and falling out of the twin-trap, while others would hover, remaining static or undulating.

A slightly oval shaped particle was more likely to levitate than a fully rounded one, even if their sizes were the same. The reason for it is related to how well the particle fits and is held between the tweezers of the trap. By gently pressing a round particle to deform it into an oval, a non-floating particle would achieve levitation.

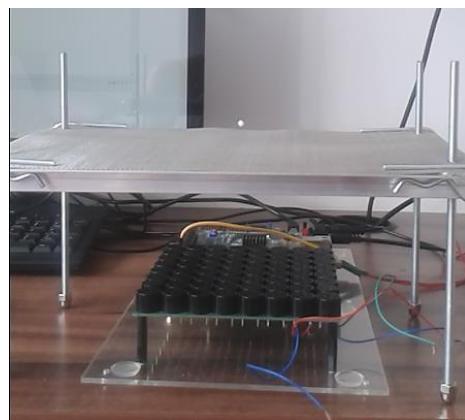


Figure 46: Polystyrene sphere levitating above an acoustically transparent mesh

The mesh fixture was removed and mid-air levitation was obtained with particles that had exhibited good stability using the mesh. Some particles that were capable of levitating in the presence of the mesh were not able to do so without it. In contrast, any particle levitating without the mesh would levitate with the mesh as well.



Figure 47: Mid-air levitation of polystyrene sphere (side view)

Levitation was achieved for particles with the following diameters: 2.5 mm, 3 mm, 3.5 mm, 4 mm, 4.5 mm, and 5 mm.

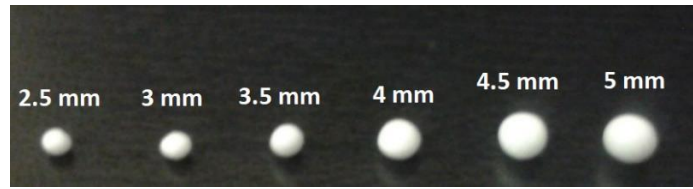


Figure 48: Diameters of levitated particles

The particle was able to levitate without falling using the minimum coordinates of (31,31,100) and the maximum coordinates of (93,93,100). The approximate stable levitating area is shown below.

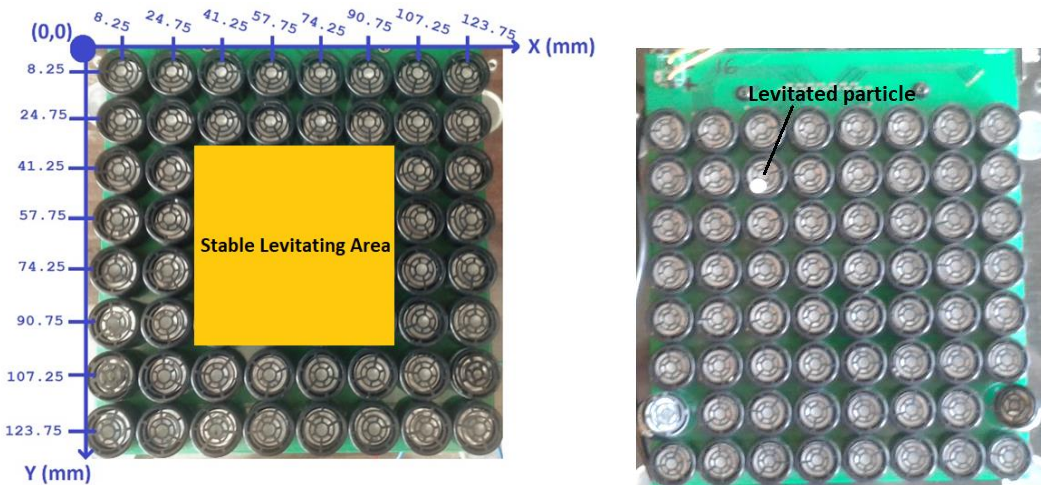


Figure 49: Stable levitating area for a 4 mm particle

6.3 Particle transportation

To test the ability of the phased array to transport a 4 mm particle with the acoustic twin-trap as well as to determine the maximum average speed achieved without the particle falling, the focal point was moved in small increments along the Y axis, while maintaining the X axis constant, and vice versa. The collection of figures below shows the movement of the particle in the Y axis.



Figure 50: Translation of 4 mm sphere along Y axis with 1 mm step size (top view)

A specific test consisted in moving the sphere in a straight line from coordinates (60,66,100) to (69,66,100) and then back to the starting point. At each step taken, a delay was introduced to help the particle stabilize to its new position. The average speed was calculated as the total distance travelled (18 mm) divided by the total time taken to arrive back at the starting point. This test was performed twice for different step sizes, reducing the delay per step to determine the maximum speed.

A minimum step size of 1 mm allowed a stable translation of the particle at a maximum average speed of 5 mm/second along a total distance of 18 mm. A maximum step of 2.5 mm permitted transporting the same particle at 1 mm/second.

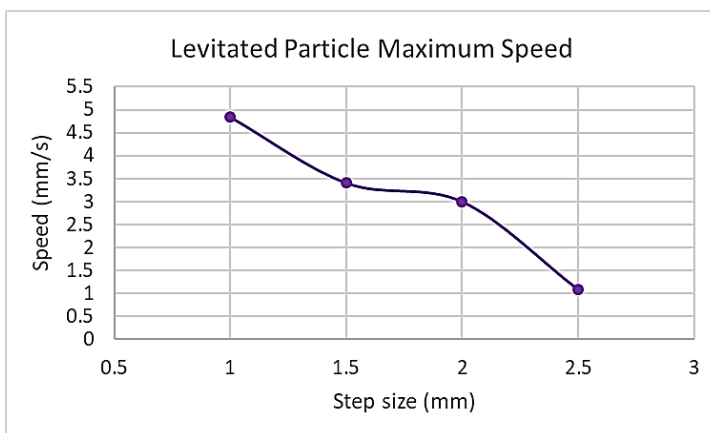


Figure 51: Levitated 4 mm particle maximum speed

6.4 Captured echoes

The following graphs present an example of the echoes that were captured by both receivers with a levitated particle moving along the X axis, while keeping Y = 66 and Z = 100.

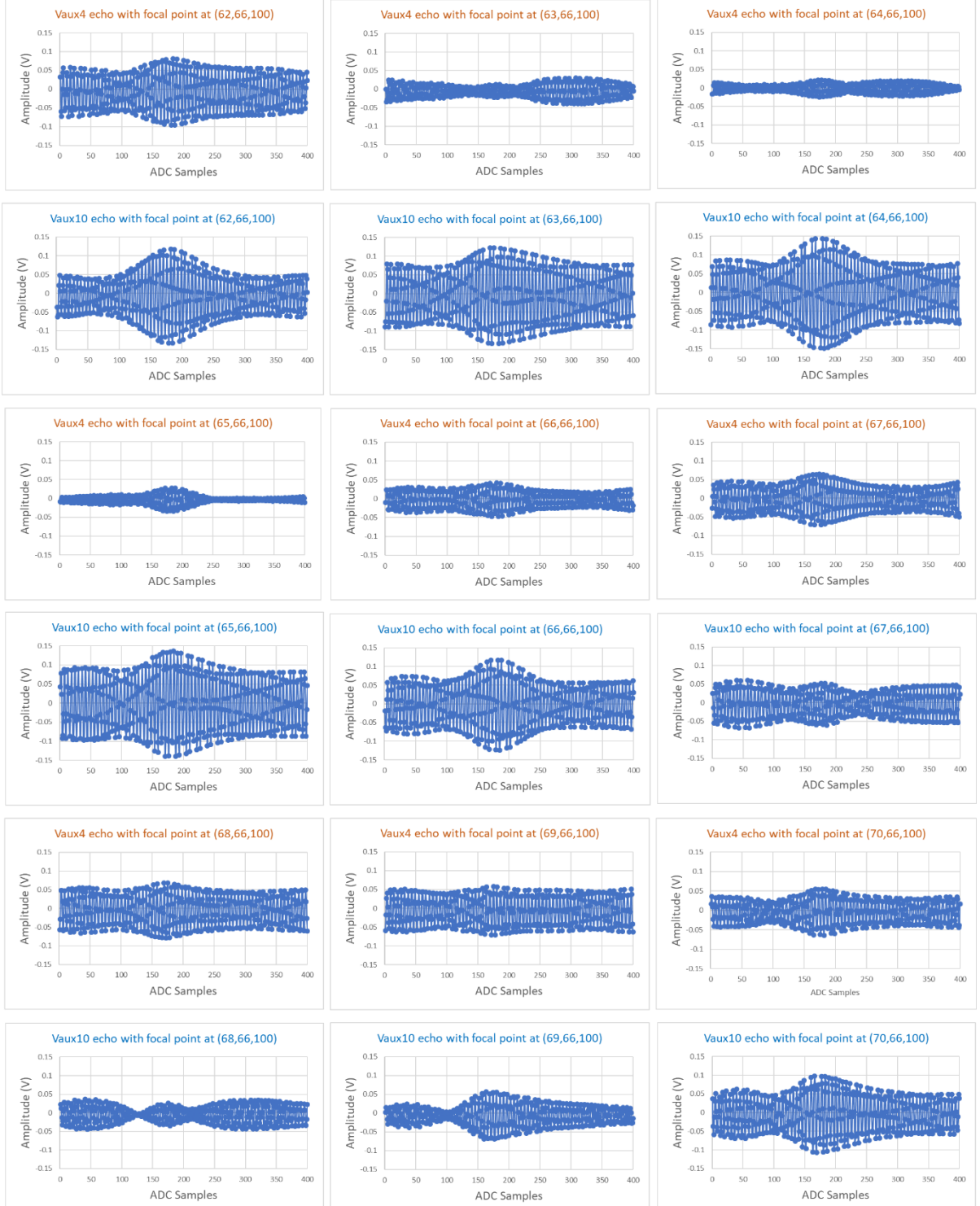


Figure 52: Echo waves for X coordinate 62 to 70 and Y coordinate 66

The following graphs present an example of the echoes that were captured by both receivers with a levitated particle moving along the Y axis, while keeping X = 66 and Z = 100.

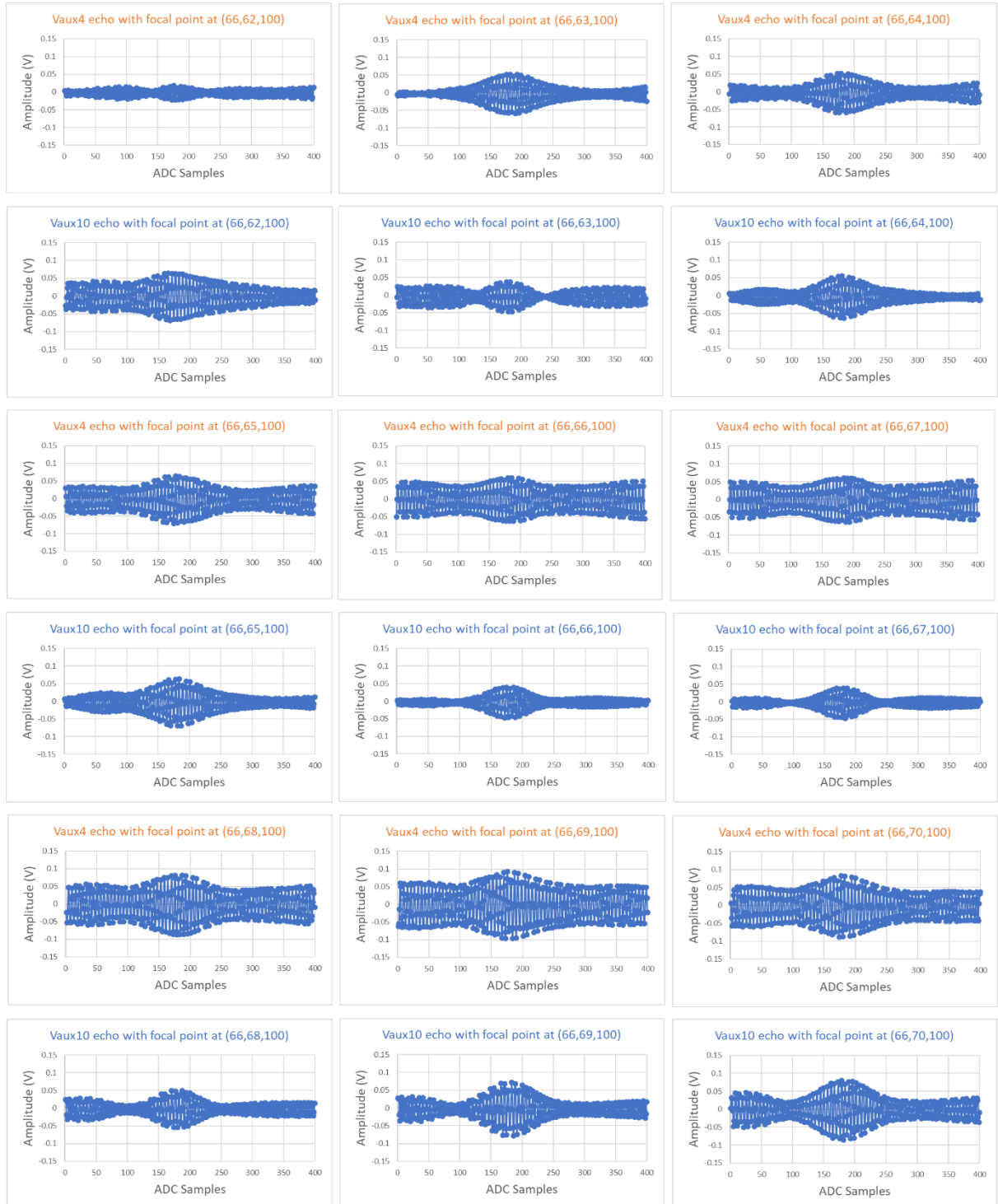


Figure 53: Echo waves for X coordinate 66 and Y coordinate 62 to 70

6.5 Particle position analysis

Using the statistical method for estimating particle position, described in Section 5.2.5.2, it was necessary to establish ranges at which peak values occur for each X coordinate, since echoes vary from one measurement to the next. It was also observed that some coordinates share the same peak value ranges, making it difficult to discern between coordinates.

The graphs below show the ADC sample number ranges versus the percentage of times the echo's peak value fell in that range.



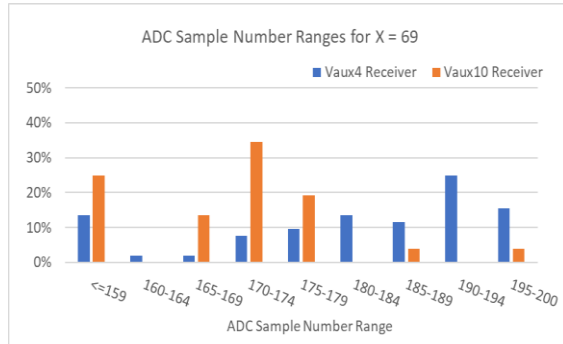


Figure 54: Particle position statistical analysis along the X-axis

From the graphs, it is difficult to discern one coordinate from another. However, the following table summarizes the probable X coordinates for each range.

ADC Sample Number Range	Probable X coordinates
<=159	63,64,65,69
160 to 164	Undefined
165 to 169	67,68,69
170 to 174	64,67,68,69
175 to 179	Undefined
180 to 184	Undefined
185 to 189	64,65,66,67
190 to 194	64,65,68,69
195 to 200	Undefined

Table 6: Probable X coordinate within ADC sample number range

6.6 Echo amplitude test

An echo amplitude test was performed using cardboard and foam squares, with the side of the square ranging from 4 mm to 50 mm. The purpose of this test was to determine how the size and material of the object affect the echo amplitude observed by the two receivers.

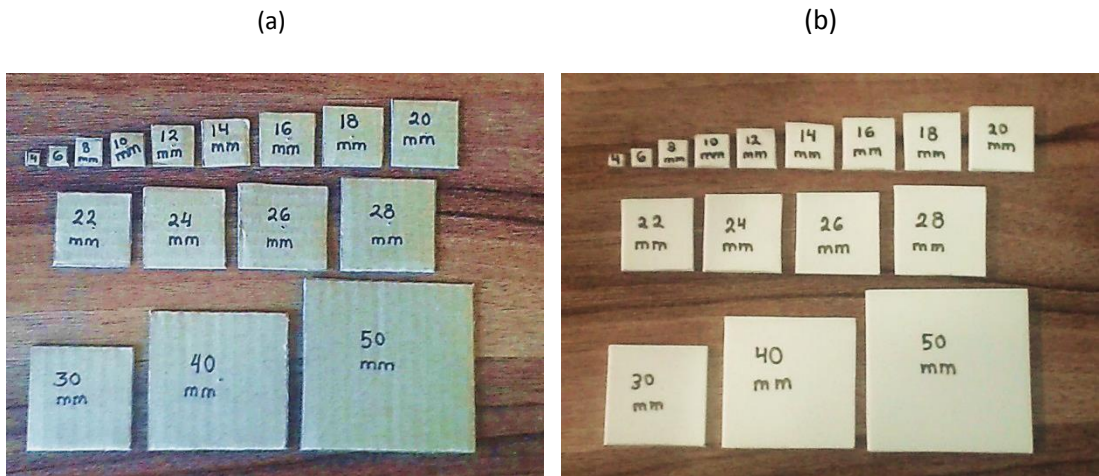


Figure 55: Carboard (a) and foam (b) squares for echo amplitude test

Each square was suspended at a height of 100 mm from the center of the phased array using a pin hanging from a string. A focal point was created at the center coordinate (66,66,100), and both receivers were enabled.

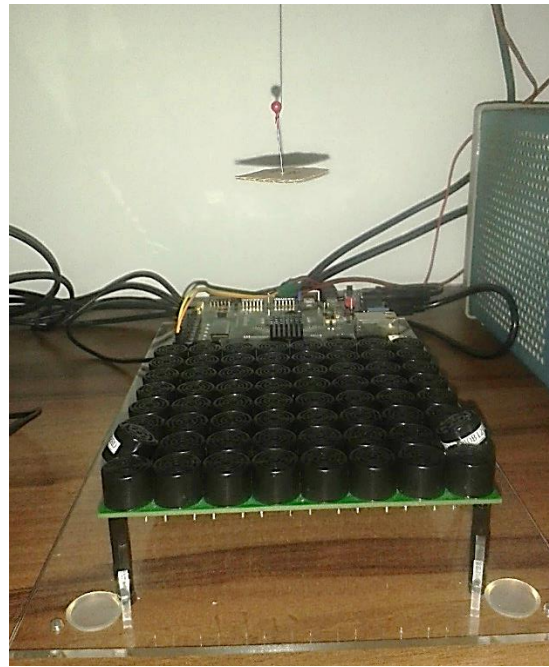


Figure 56: Echo test setup with carboard and foam squares

The following graph presents the overall peak amplitude captured by the receivers for each square size. The minimum amplitude recorded using a square of 4 mm per side was approximately 160 mV. For squares above 30 mm per side, this amplitude reached the ADC saturation value of 500 mV.

The trend of the waveforms does not follow a linear behavior. The reason for it is that a high echo amplitude is the result of a good line of sight between the transmitter and the object as well as the echo being reflected at the correct angle to reach the receiver. The size of the

object increases the probability of the acoustic wave to hit the object and bounce back, but the angle at which it is reflected is also important. Therefore, the orientation of the object matters. It was observed that even with a small particle it was possible to receive a high echo amplitude when oriented correctly.

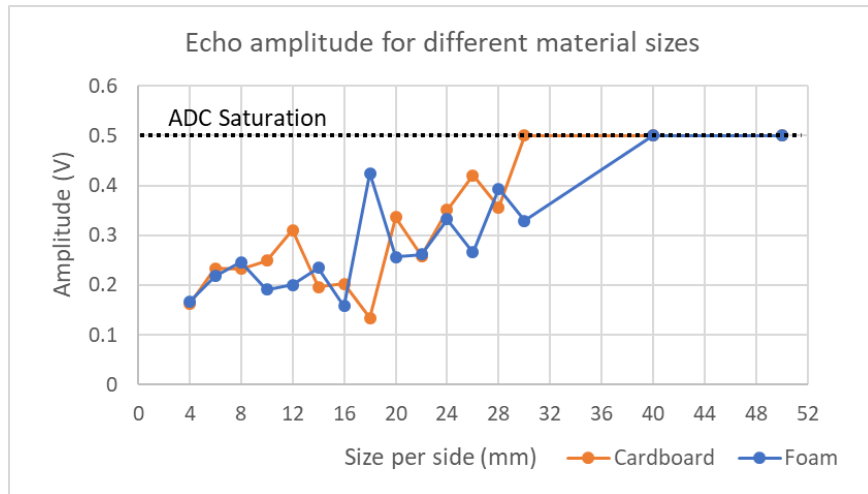


Figure 57: Echo amplitude for different material sizes

6.7 System Response to the presence of objects

A maximum amplitude of 110 mV was captured at the receivers for a particle of 4 mm diameter, when the particle levitates between coordinates (63,66,100) and (69,66,100). This maximum voltage was recorded for this specific array setup, and would be different if the echo receivers were located at a different position.

100 mV was used as a threshold value to determine the absence or presence of other objects in the way, apart from the levitated particle. Response of the system to echo peak amplitudes higher than this value was introduced by moving the particle away from the receiver which recorded the echo above threshold. If the threshold was not surpassed, the particle remained in the same position.

The response of the system was tested using a cardboard square of 50 mm per side, which had proved to generate echo amplitudes above the threshold voltage. The cardboard square was placed close to the focal point from the left and right sides of the phased array, to create large echoes on Vaux4 and Vaux10, respectively. This caused the particle to move in the opposite direction of the cardboard square along the X axis, confirming the ability to establish a feedback response based on echo reception.

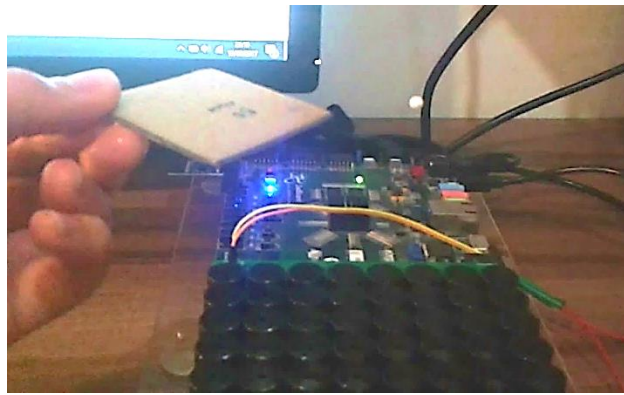


Figure 58: System response to presence of objects

7. CONCLUSIONS

Single-sided beam levitation was achieved with an FPGA-based ultrasonic phased array driver using an acoustic trapping mechanism. This trap was generated as a combination of a beam focusing action to create a focal point and a phase signature added to it.

Feedback was added to the system by converting two of the original transmitters on the phased array into receivers. Echo waves reflected from the levitated particle were captured and used for position estimation and system response. Position estimation was not entirely achieved as a result of the limited number of receivers and the small size of the particle not being able to reflect the acoustic waves properly. Both size and orientation of an object influence the echo amplitude detected by the receivers.

There are several factors that affect levitation, including the shape and size of the levitated object, as well as the temperature, pressure, and humidity of the environment, which influence the speed of sound and its wavelength.

A temperature sensor was included in the design to correct for temperature variations affecting the speed of sound value.

8. FUTURE WORK

The proposed tasks to enhance the work described are listed below:

- 1) System identification of the phased array to obtain a model that can be used for closed loop control. It may be necessary to model the individual response of the ultrasonic transducers as well as the response of the combined transducer array.
- 2) Design and implementation of a PID controller within the SoC platform to drive the transducer array.
- 3) Simulation of the closed loop system in MATLAB/Simulink.
- 4) Improvement of the phased array using smaller transducers for greater accuracy, as well as more receivers for better echo wave feedback. Potentially use transceiver components that permit the transducer elements to act both as transmitters and receivers.
- 5) Use MOSFET drivers that allow for higher output voltages with the purpose of levitating heavier objects.
- 6) Enable the ability of the phased array to control the levitated object in 3D, not only varying the XY-plane but also the focal length.
- 7) Experiments with other acoustic trapping mechanisms, including vortex and bottle traps.

9. REFERENCES

- [1] Laurell T. Acoustophoresis | Biomedical Engineering [Internet]. Bme.lth.se. 2016 [cited 13 September 2017]. Available from: <http://bme.lth.se/research-pages/nanobiotechnology-and-lab-on-a-chip/research/acoustophoresis>
- [2] Long B, Seah SA, Carter T, Subramanian S. Rendering volumetric haptic shapes in mid-air using ultrasound. ACM Transactions on Graphics (TOG). 2014 Nov 19;33(6):181.
- [3] Ochiai Y, Kumagai K, Hoshi T, Hasegawa S, Hayasaki Y. Cross-field aerial haptics: Rendering haptic feedback in air with light and acoustic fields. In Proceedings of the 2016 CHI Conference on Human Factors in Computing Systems 2016 May 7 (pp. 3238-3247). ACM.
- [4] Hoshi T. Noncontact Tactile Display Using Airborne Ultrasound.
- [5] Assef AA, Maia JM, Costa ET. Initial experiments of a 128-channel FPGA and PC-based ultrasound imaging system for teaching and research activities. In Engineering in Medicine and Biology Society (EMBC), 2016 IEEE 38th Annual International Conference of the 2016 Aug 16 (pp. 5172-5175). IEEE.
- [6] Lu Y, Ahn IS, Smith R. FPGA-based ultrasonic signal processing platform. In Electro Information Technology (EIT), 2016 IEEE International Conference on 2016 May 19 (pp. 0610-0614). IEEE.
- [7] Gilliland S, Govindan P, Gonnot T, Saniie J. Performance evaluation of FPGA based embedded ARM processor for ultrasonic imaging. In Ultrasonics Symposium (IUS), 2013 IEEE International 2013 Jul 21 (pp. 519-522). IEEE.
- [8] Bucher I, Ilssar D, Gabai R, Cohen N, Shaham R, Davis S. Controlled acoustic levitation—physical model and real-time digital implementation. In Advanced Intelligent Mechatronics (AIM), 2016 IEEE International Conference on 2016 Jul 12 (pp. 452-456). IEEE.
- [9] Denes PB, Pinson EN. The Speech Chain: The Physics and Biology of Spoken Language (1963) Murray Hill. NJBell Telephone Laboratories.
- [10] Diatkine C. Introduction - Waveform Introduction [Internet]. Support.ircam.fr. 2011 [cited 13 September 2017]. Available from: <http://support.ircam.fr/docs/AudioSculpt/3.0/co/Acoustic%20Notions.html>
- [11] Schmerr Jr LW. Fundamentals of ultrasonic phased arrays. Springer; 2014 Aug 13.
- [12] Nelligan T, Kass D. Intro to Ultrasonic Phased Array | Olympus IMS [Internet]. Olympus-ims.com. [cited 13 September 2017]. Available from: <http://www.olympus-ims.com/sv/ultrasonics/intro-to-pa/>

- [13] Wang H. Development of Electronic Systems for Ultrasonic Particle Manipulation (Doctoral dissertation, University of Dundee, Scotland).
- [14] Lamarre A, Mainguy F. Dynamic focusing of phased arrays for nondestructive testing: characterization and application. In Proceedings of the international symposium on advanced sensors for metals processing 1999.
- [15] Nakahata K, Kono N. 3-D modelings of an ultrasonic phased array transducer and its radiation properties in solid. In Ultrasonic Waves 2012. In Tech.
- [16] Olympus Phased Array Tutorial, Learn About Ultrasonic Phased Array [Internet]. Olympus-ims.com. [cited 13 September 2017]. Available from: <http://www.olympus-ims.com/en/ndt-tutorials/phased-array/>
- [17] Nakahata K, Kono N. 3-D modelings of an ultrasonic phased array transducer and its radiation properties in solid. In Ultrasonic Waves 2012. InTech.
- [18] Smith SW, Pavly HG, von Ramm OT. High-speed ultrasound volumetric imaging system. I. Transducer design and beam steering. IEEE transactions on ultrasonics, ferroelectrics, and frequency control. 1991 Mar;38(2):100-8.
- [19] Ochiai Y, Kumagai K, Hoshi T, Hasegawa S, Hayasaki Y. Cross-field aerial haptics: Rendering haptic feedback in air with light and acoustic fields. In Proceedings of the 2016 CHI Conference on Human Factors in Computing Systems 2016 May 7 (pp. 3238-3247). ACM.
- [20] Ochiai Y, Hoshi T, Rekimoto J. Pixie dust: graphics generated by levitated and animated objects in computational acoustic-potential field. ACM Transactions on Graphics (TOG). 2014 Jul 27;33(4):85.
- [21] Acoustic tweezers | Wikiwand [Internet]. Wikiwand. [cited 13 September 2017]. Available from: http://www.wikiwand.com/en/Acoustic_tweezers
- [22] Godin OA. Rayleigh scattering of a spherical sound wave. The Journal of the Acoustical Society of America. 2013 Feb;133(2):709-20.
- [23] Lapin AD. Scattering of a Rayleigh wave by monopole-dipole resonators. Acoustical Physics. 2007 Feb 1;53(1):11-5.
- [24] Wilson T. How Acoustic Levitation Works [Internet]. HowStuffWorks. [cited 13 September 2017]. Available from: <http://science.howstuffworks.com/acoustic-levitation1.htm>
- [25] Sound Wave Interference [Internet]. Sound-physics.com. [cited 13 September 2017]. Available from: <http://www.sound-physics.com/Sound/Interference>
- [26] Valverde JM. Acoustic streaming in gas-fluidized beds of small particles. Soft Matter. 2013;9(37):8792-814.

- [27] Acoustic Levitation - Levitation of single solid or liquid samples in in ultrasonic single ultrasonic single-axis standing axis standing-wave levitators [Internet]. Paul Scherrer Institut - Laboratory for Developments and Methods [cited 13 September 2017]. Available from: https://www.ill.eu/fileadmin/users_files/documents/instruments_and_support/sample_environment/Events/Levitation_Workshop/PSI.pdf
- [28] Vandaele V, Lambert P, Delchambre A. Non-contact handling in microassembly: Acoustical levitation. *Precision engineering*. 2005 Oct 31;29(4):491-505.
- [29] Liu P, Li J, Ding H, Cao W. Modeling and experimental study on near-field acoustic levitation by flexural mode. *IEEE transactions on ultrasonics, ferroelectrics, and frequency control*. 2009 Dec;56(12).
- [30] Marzo A, Seah SA, Drinkwater BW, Sahoo DR, Long B, Subramanian S. Holographic acoustic elements for manipulation of levitated objects. *Nature communications*. 2015 Oct 27;6.
- [31] Design MB. Vivado Design Suite User Guide. 2012.
- [32] SDx Environments Release Notes, Installation, and Licensing Guide [Internet]. Xilinx; 2016 [cited 13 September 2017]. Available from: https://www.xilinx.com/support/documentation/sw_manuals/xilinx2016_3/ug123-8-sdx-rnil.pdf
- [33] ZedBoard (Zynq™ Evaluation and Development) Hardware User's Guide [Internet]. Avnet; 2014 [cited 13 September 2017]. Available from: http://zedboard.org/sites/default/files/documentations/ZedBoard_HW_UG_v2_2.pdf
- [34] ZedBoard | Zedboard [Internet]. Zedboard.org. [cited 13 September 2017]. Available from: <http://zedboard.org/product/zedboard>
- [35] Marzo A, Corkett T, Drinkwater B. Ultraino: An Open Phased-Array System for Narrowband Airborne Ultrasound Transmission.
- [36] AXI XADC Core [Internet]. Xilinx.com. 2017 [cited 13 September 2017]. Available from: https://www.xilinx.com/products/intellectual-property/axi_xadc.html
- [37] Sengpiel E. Calculation speed of sound in humid air and the air pressure humidity moist air water vapor density of water atmospheric pressure - sengpielaudio Sengpiel Berlin [Internet]. Sengpielaudio.com. [cited 13 September 2017]. Available from: <http://www.sengpielaudio.com/calculator-airpressure.htm>
- [38] Sensor P. Pmod HYGRO: Digital Humidity and Temperature Sensor [Internet]. Digilent. [cited 13 September 2017]. Available from: University of Bristol

- <http://store.digilentinc.com/pmod-hygro-digital-humidity-and-temperature-sensor/>
- [39] Taylor A. Adam Taylor's MicroZed Chronicles, Part 188: Pmods! [Internet]. Forums.xilinx.com. 2017 [cited 13 September 2017]. Available from: <https://forums.xilinx.com/t5/Xcell-Daily-Blog/Adam-Taylor-s-MicroZed-Chronicles-Part-188-Pmods/ba-p/762097>
- [40] Taylor A. MicroZed XADC Software: Adam Taylor's MicroZed Chronicles Part 8 [Internet]. Forums.xilinx.com. 2013 [cited 13 September 2017]. Available from: <https://forums.xilinx.com/t5/Xcell-Daily-Blog/MicroZed-XADC-Software-Adam-Taylor-s-MicroZed-Chronicles-Part-8/ba-p/383861>
- [41] ZedBoard Schematic - Xilinx [Internet]. Xilinx; 2013 [cited 13 September 2017]. Available from: https://www.xilinx.com/support/documentation/university/XUP%20Boards/XUPZedBoard/documentation/ZedBoard_RevC.1_Schematic_130129.pdf
- [42] 7 Series FPGAs and Zynq-7000 All Programmable SoC XADC Dual 12-Bit 1 MSPS Analog-to-Digital Converter User Guide [Internet]. Xilinx; 2016 [cited 13 September 2017]. Available from: https://www.xilinx.com/support/documentation/user_guides/ug480_7Series_XADC.pdf
- [43] Creating a custom IP block in Vivado Using ZedBoard: A Tutorial - Embedded Processor Hardware Design [Internet]. 2015 [cited 13 September 2017]. Available from: http://islab.soe.uoguelph.ca/sareibi/TEACHING_dr/XILINX_VIVADO_dr/VivadoEmbeddedZyncTutorialAddIP.pdf
- [44] Johnson J, Johnson J. Creating a custom IP block in Vivado | FPGA Developer [Internet]. Fpgadeveloper.com. 2014 [cited 13 September 2017]. Available from: <http://www.fpgadeveloper.com/2014/08/creating-a-custom-ip-block-in-vivado.html>

10. APPENDIX

Available supplementary .mov videos:

Video Name	Description	Duration	Size
Move in XY plane - 1 sec delay	The particle is moved along the XY-plane using a step size of 1 mm and with a 1 second delay between steps taken.	1:15 min	224 MB
Move in XY plane - 300ms delay	The particle is moved along the XY-plane using a step size of 1 mm and with a 300 ms delay between steps taken.	1:38 min	286 MB
Echo feedback control.mov	A cardboard square is placed beside the levitated particle for the system to react, moving the particle away from the cardboard.	3:14 min	491 MB
Test speed	A particle is moved at different speeds along the X-axis.	2:18 min	323 MB

Table 7: List of available videos